AN INVESTIGATION OF THE DYNAMIC CHARACTERISTICS OF A HARD DISK DRIVE BY EXPERIMENT AND ANALYSIS

Q. H. Zeng and D. B. Bogy

Computer Mechanics Laboratory

Department of Mechanical Engineering

University of California

Berkeley, CA 94720

August, 1996

CONTENTS

AN INVESTIGATION OF THE DYNAMIC CHARACTERISTICS OF A HARD DISK DRIVE BY EXPERIMENT AND ANALYSIS

Q. H. Zeng[1] and D. B. Bogy

Computer Mechanics Laboratory

Department of Mechanical Engineering

University of California

Berkeley, CA 94720

ABSTRACT

This report presents an investigation of the dynamic characteristics of a commercially available hard disk drive using both experimental and numerical techniques. The drive has a storage capacity of 1GB with two $3^1/_2$ inch disks. First, each individual component - disk, suspension assembly, actuator arm, and arm coupled with the assembly - was studied. Next, modal experiments were performed of the system in both states with the disks stationary and rotating. The power spectra of the drive's vibration were measured when the drive was in operation. Finally, an FE model of the drive was created. The model consists of one disk, two actuator arms and two suspension assemblies. Good correlation between the experiment and FE analysis was achieved. It was shown that the drive exhibits very complicated modal properties, and there are primarily four types modes; strong suspension modes, strong arm-suspension modes, strong disk modes, and coupled modes. The actuator arm significantly affects the dynamics of the drive, especially during track-seeking.

---

[1] Visiting scholar, Associate professor, Institute of Vibration Engineering, Nanjing University of Aeronautics & Astronautics, Nanjing, China.

1. INTRODUCTION

Magnetic hard disk drives are continually made smaller in size, higher in capacity and lower in cost, and are now the most important means of information storage. The drives contain high performance electromechanical components, which consist of one or more rotating disks coated with thin layers of magnetic material and rotated by a spindle motor, an array of suspension assemblies that include sliders (housing the read/write transducers), flexures and loadbeams, and actuators driven by a voice-coil motor. Data are stored in the magnetic layers of the disks in bit cells along concentric tracks that can be accessed by the actuators.

The areal density, which information storage technology strives to increase, is determined by the track density and bit cell (linear) density. Linear density depends on the flying height between the sliders and the magnetic media, and the relative speed between the transducers and the media. The speed is determined by the disk rotation speed and radial position of the sliders. Current drives have flying heights below 80 nm and over 5000 RPM disk rotating speed. The track density is mainly limited by vibration of the electromechanical components and the servo control system. The current drives have track densities approaching 7000 TPI, which means that the positioning errors between the sliders and disks in the radial direction should be less than 20 μin. Besides the requirement of high-accuracy positioning, high-speed positioning is also critical. The positioning speed is limited by the residual vibration, which occurs after the track seeking motion. Reliability of the drives under operating and non-operating mechanical disturbance has come into currency due to the advent of the portable lap-top computers.

All of these requirements are directly related to the dynamic behavior of the electromechanical components and systems in the drives. To further increase the density, access speed and reliability, a thorough understanding of this behavior is extremely important. There are many works devoted to the electromechanical components and systems through experiments, analysis and designs. However, most of the available literature focuses on the individual components. For example, McAllister (1996) investigated the effect of platter resonances on track misregistration by experiments, and found that the axial vibration of the disks produces a significant amount of the track misregistration at 7200 RPM. Ku (1996) studied dynamic characteristics of the spindle motors, and compared ball bearings with hydrodynamic bearings. Yoshida et al. (1995) presented a new design of the actuators to reduce the residual vibration. Zeng and Bogy (1996b) studied dynamic properties of the Type 850AK suspension assembly through modal experiments and finite element (FE) analysis.

When the individual components are integrated into a system, they interact with each other, and exhibit more complicated properties. However, few research works on the dynamics of the system are found. Those available mainly focus on the following aspects. Radwan and Whaley (1993) researched servo-structure interaction using FE analysis, and built FE models of the actuators and suspension assemblies to analyze the effect of assembly/actuator resonance on the open-loop servo response of the drive. Wilson and Bogy (1994) performed modal experiments of an IBM 3380 suspension loaded on a $5^1/_4$ inch rotating disk, and found that when a natural frequency of the suspension is close to

that of the disk, two resonant frequencies are created when the components are coupled together. They (Wilson and Bogy, 1993) also carried out an experimental modal analysis of the Type 1650 suspension / disk (90 mm) system, and showed that the coupled system exhibits strong disk modes, strong suspension modes and coupled modes.

The complete drives are much complicated than these examples that have been studied. In this report, dynamic properties of a commercially available $3^1/_2$ inch drive (1GB capacity) was investigated by experiments and FE analysis. First, each component was individually modeled. Next, modal experiments were performed in both states with the disks stationary and rotating. Power spectra of the drive's vibration were measured when the drive was in operation. Finally, an FE model of the system was created. The model consists of one disk, two actuator arms and two suspension assemblies. Good correlation between the experiment and FE analysis was achieved. It was shown that the drive exhibits very complicated modal properties, and the actuator arm plays an important role in the dynamics of the drive.

2. HARDWARE DESCRIPTION

The hardware to be studied in this report is a commercially available hard disk drive. The drive consists of two 95 mm disks rotated by a fixed shaft spindle motor, four 850AK suspension assemblies (four 50% tripad sliders), three actuator arms that are driven by a voice coil motor, and a base/cover. When power is applied, the disks rotate at 5200 RPM. The slider flies over the surface of the disk on an air bearing generated by the relative motion between the rotating disks and the stationary sliders.

We attempted to understand the dynamical properties of the full drive. Any structural modification of the drive would change these properties. Therefore, the modifications were kept to a minimum. Except for cutting a small window in the cover, as shown in Figure 1, no modification was made. The radial position of the sliders was varied from about 19 mm to 44 mm from the center of the spindle. The excitation was applied through the window to the upper actuator arm, and the vibration of the upper suspension and disk were measured.

3. EXPERIMENTAL SETUP

Figure 2 shows a schematic representation of the experimental system utilized in the study. The system was totally described and verified in Zeng and Bogy (1996a). The electromagnetic excitation method was chosen to excite the drive. The electromagnetic exciter (Type B) and power amplification circuit (Wilson and Bogy, 1996) were used to generate a non-contact excitation force. A ferromagnetic target was required. The target was attached to the actuator arm by use of adhesive. The level of the excitation force highly depends on the working gap between the exciter and the target. The exciter was mounted onto a Z stage to easily adjust the gap. In the experiment, the gap was adjusted through trial and error based on the measured excitation and response signals. The drive was mounted on an XY stage to conveniently position the excitation point.

A force sensor (PCB model 209A) was mounted between the exciter and the Z stage to measure the excitation force. A Polytec Laser Doppler Vibrometer (LDV) was used to

measure the absolute velocity responses of the components. The LDV was supported by an XYZ stage to permit convenient changing of the measurement points. An HP3562A Dynamic Signal Analyzer was adopted for data acquisition and analysis to obtain the frequency response functions (FRFs) between the velocity responses and the excitation force. Burst random and chirp signals were used in the excitation. A miniature PCB force hammer was also used to excite the disks to measure the disk resonances. The enhanced modal analysis software NAI-MODAL was applied in the geometric modeling of the assembly, controlling the analyzer, reading FRFs from the analyzer and storing FRFs and measurement parameters into a database, as well as curve fitting, mode sorting, and mode shape animation. The function of the multiple frequency band measurement in the experimental system dramatically reduces the time consuming work.

4. EXPERIMENTS AND ANALYSIS OF THE COMPONENTS

To accurately and reliably create the model of the drive and better understand its properties, we preliminarily modeled each individual component by analysis and experiment. The major components in our research are the disks, suspension assembly and actuator arms.

4.1 Experiments and Analysis of the disk

4.1.1 Experiments in its free state. The geometry of the disk is very simple, so only the modal frequencies of the disk were measured in its free state. The disk was supported by very soft sponges to simulate the free state. The outer diameter of the disk was impacted with the force hammer in that axial direction while the velocity response was measured at

the outer diameter of the disk in the direction with the LDV. The modal frequencies were found from the FRFs computed by the Analyzer. The frequencies are shown in Table 1.

4.1.2 FE analysis of the disk in its free state. The disk is an aluminum-magnesium substrate platter. The following parameters were used to create an FE model.

Dimensions: Outside diameter 95 mm, Inside diameter 25 mm, Thickness .8 mm

Material properties: Young's modulus 73 GPa, Mass density 2770 kg/m^3 , Poisson's ratio 0.33

Using the ANSYS FE code, an FE model was created, as shown in Figure 3. The model consists of 1600 shell elements (Shell63), and 10104 active DOFs. The modal frequencies were calculated and are shown in Table 1. From Table 1, we can see that the calculated results are almost always larger than the experimental results. These biased differences could mainly come from errors of the material properties of the disk used in the FE analysis. Because there are magnetic and lubricant layers on the disk, the density of the disk would be larger than the one used for the aluminum. Based on the differences, the density was updated to 2770*1.05 kg/m^3 . Then, considering the manufacturing tolerances of the dimensions, the dimensions were updated by the ANSYS design optimization. The dimensions were defined as design parameters, and the objective function was defined as

$$\varepsilon = \sum_{m=1}^{9} r \times \left[\left(f_m^A - f_m^M \right) / \, f_m^M \right]^2 \qquad (1)$$

where f_m^A and f_m^M are analyzed and measured modal frequencies, respectively, and r is the repeated number of the mode (1 or 2). The model was automatically updated. The updated dimensions are as follows.

Outside diameter 94.937 mm, Inside diameter 24.905 mm, thickness .80138 mm. The modal frequencies calculated from the updated model are shown in Table 1, where $(m, n)^r$ is used to define the mode shapes of the disk; m, n, and r represent the number of nodal circles, the number of nodal diameters, and the repeated number of the mode, respectively. Table 1 shows the calculated modal frequencies of the modes $(0, n)^2$ are larger than the experimental results, and the calculated modal frequencies of the modes (m, 0) and (1, n) are less than the experimental results. This may imply the disk is exhibiting a small non-isotropic property. The largest difference between experiment and analysis is less than 2.4%.

The model of the disk in Figure 3 is not suitable to analyze the drive because the mesh in the region coupled with the sliders is not fine enough, and the number of the DOFs is too large. Therefore, another model was created and is shown in Figure 4. The model consists of 568 shell elements and 3456 active DOFs. The mesh in the region interfaced with the sliders are very fine. The modal frequencies calculated from the two models are very close to each other. Only the second model will be used in the later analysis.

4.1.3 Experiments in the drive. In the drive, the disks are clamped at the inner diameter of about 32 mm. To determine the frequencies, a similar experiment was performed. The sliders were fixed at the inner limitation diameter. The upper disk was impacted with the hammer, and the responses were measured. The FRFs were obtained by the Analyzer.

The frequency range of 0-4.5 kHz was divided into many sub-ranges to obtain good frequency resolutions. As example, Figure 5 shows three measured FRF curves. The first peak in the first curve, at about 534 Hz, might be the mode of the entire disk pack rocking on the bearing (Frees, 1995). The second resonance, at about 570 Hz, is a coupled mode related to the actuator arm and suspension, which will be discussed later. The curves show two very close peaks in some frequency ranges, which could be caused by two disks in the drive and/or a small asymmetry of the disks. From the peaks of the FRFs, the modal frequencies were determined, and shown in Table 2. To check the effect of the location of the sliders on the frequencies, the sliders were moved to the outer limitation diameter. The frequencies were measured again. The frequency changes are less than 1%. Therefore, the sliders' location does not significantly affect the dynamic properties of the drive.

4.1.4 FE analysis of the disk in the drive. The second FE model of the disk in its free state was used to analyze its properties in the drive. The boundary condition of the clamped inner radius should be modeled. To simplify the analysis, the clamped inner radius of the disk was modeled as nodal points restrained to zero displacement. The outer clamped radius is about 16.33 mm. Considering the contribution of the flexibility of the hub, the clamped radius in the model should be between 12.5 mm and 16.33 mm. The clamped radius of 15.1427 mm was found through trial and error based on the frequency differences between analysis and experiment. The calculated modal frequencies are shown in Table 2. The maximum difference between experiment and analysis is less

2.2%. That means that the model can probably simulate the dynamic properties of the disk efficiently well.

When the disk is rotating, there is a centrifugal force field acting on the disk, which will increase the stiffness of the disk. To predict its effect on the modal frequencies, the prestressed modal analysis was performed. The modal frequency changes of the (m, n) modes for the prestressed effects were found and are shown in the Table 2. The modal frequencies increase about 10 Hz for each mode due to the prestressed effects. For example, when the disk is rotating, the frequency of mode (0, 1) will be increased from 603.5 Hz to 613.9 Hz due to the prestressed effects..

Some mode shapes are shown in Figure 6. From the symmetry of the disk, each modal frequency of mode $(m, n)^r$ $(n>0)$ has two orthogonal mode shapes. In the practical analysis and experiment, the disk is not perfectly symmetric, and the two mode shapes will correspond to two close modal frequencies, respectively.

4.2 Analysis of the Suspension Assembly in its Loaded State

The suspension assembly with a through-etch radius was exhaustively investigated through experiment and analysis, and an FE model of the assembly was created and validated by the experiments reported in Zeng and Bogy (1996b). The assembly used in the drive has a partial-etch radius. First, the FE model was modified to include the partial-etch radius. Then. the angle $\theta=2^o$ of the rail of the loadbeam was used, and the four corners of the slider were constrained with zero displacement in the Z direction to model

the loaded state. The FE model is shown in Figure 7. The model consists of 1305 shell elements (Shell63), 12 solid elements (Solid45), and 8687 active DOFs. The modes in the frequency range of 0-14 kHz were calculated using the subspace iteration method. The analyzed modal frequencies and mode shapes are shown in Figure 8.

4.3 Analysis of the Actuator Arm

There are three actuator arms in the drive. The arm located at the middle, on which two suspension assemblies are mounted, is thicker than the other two arms. Because the test samples and design drawings of the arms were not available, an FE model of the arm was created using only limited measured parameters. The model is shown in Figure 9. The pivot shaft (a diameter of about 6.4 mm) was modeled as nodal points restrained to zero displacement. A Young's modulus of 73 GPa, a mass density of 2770 kg/m^3 , and a Poisson's ratio of 0.33 were used as its material properties. A thickness of 0.95 mm was selected. The model consists of 1386 solid elements (Solid 73), 3774 active DOFs. The modes in the frequency range of 0-10 kHz were calculated, and are shown in Figure 10. Although the parameters in the model were approximate, and the model of the arm was not validated by experiment, we can still confirm that the modal frequencies of the first bending and sway modes of the arm are much lower than the ones of the suspension assembly, such that the arm will play an important role in the dynamics of the coupled system.

4.4 Analysis of the Arm-suspension

When the suspension assembly is attached to the actuator arm, a relatively independent coupled system, arm-suspension(AS), is constructed, and it will move together in track-seeking. Therefore, its dynamic properties were separately studied. Combining the FE model of the assembly and the actuator arm, an FE model of the AS was created. Besides the arm and the assembly, the base plate of the suspension assembly was also included in the model. The three parts were integrated together by common nodes. The entire model, shown in Figure 11, consists of 1317 shell elements, 12 Solid45 elements, 1836 Solid73 elements, and 13091 active DOFs. The first twelve modes were calculated, and are shown in Figure 12. From Figure 12, we can see that:

❶ The modal frequency of the first bending mode of the coupled system is much lower than the one of the individual assembly;

❷ The modes of the individual suspension assembly, such as the first bending, torsional modes, etc., also exist in the coupled system as local modes, with frequencies very close to the ones of the individual assembly;

❸ There are two sway modes in the coupled system, with frequencies much lower than the one of the individual assembly;

❹ There is an additional torsion mode in the lower frequency band in the system.

Based on these results, we found that the actuator arm plays a very important role in the coupled system, and strongly suggest that the coupled system, not only the assembly, should be used in the dynamic simulation, especially in the track seeking dynamic simulation.

5. MODAL EXPERIMENTS OF THE DRIVE– DISKS STATIONARY

The disks were kept stationary, and the sliders were located at the outer limitation diameter. Because of the space limitation, we could only measure the responses of the upper suspension assembly, 15% of the region of the upper disk, and the tip region of the upper actuator arm. Two experiments were made over a period of three months. Between the two experiments, a modal experiment of the drive with rotating disks was performed. The geometric model used in the experiments is shown in Figure 13. There are nine points (71-79) on the arm, nine measured points (points 91-99) on the disk, two points (points 61,62) on the slider, and six independent points (51-56) on the flexure.

5.1 The First Experiment.

In the first experiment, the excitation point was selected at the tip region of the arm, as shown in Figure 1. A small ferrotarget was glued on the point. Because of the limitation of space, only two points (71, 75) on the arm were measured. Several points on the disk, slider, flexure, and loadbeam were selected, and the preliminary measurements were made in the frequency band of 0-10 kHz. Many modes were found in this band. The highest excitation level of the system can probably only excite the modes of the drive in the band of 0-4 kHz. The modes that have larger deflection on the arm and loadbeam could also be excited beyond this band. The burst random signal is preferable in the experiment of the non-rotating drive because there are Coulomb dampings between the sliders and the disks. However, the signal can only excite the modes in the lower frequency band because of the limitation of the excitation energy. Therefore, the periodic

chirp signal that has a higher excitation energy was used, and it could excite the modes in the higher frequency band.

After the preliminary measurements, the frequency range of 0-10 kHz was divided into five frequency bands: 420-1220 Hz, 1750-2150 Hz, 2680-3080 Hz, 3900-5900 Hz, and 5700-10700 Hz. The burst random signal was used in the first band, and the periodic chirp signal was used in the remaining bands. For each band, forty-four FRFs were measured in the Z direction under the control of the software. The global orthogonal rational fractional polynomial method was chosen to perform the curve fitting. The modal parameters were obtained by mode sorting.

5.2 The Second Experiment.

In the second experiment, the excitation point was selected at the middle of the arm, as shown in Figure 1. Another ferrotarget was glued on that point. The responses of the six points (71, 75-79) on the arm were measured. Furthermore, the response of the slider in the lateral direction was also measured. The frequency range was divided into four frequency bands: 420-1220 Hz, 1750-3000 Hz, 3500-5100 Hz, 5100-10100 Hz. Following a similar procedure as before, another set of experimental results was obtained.

5.3 Experimental Results and Discussion.

Very similar results were obtained from the two experiments. Figure 14 shows the measured FRFs in the band of 420-1220 Hz. The averaging FRFs show that there are at least six modes in the band. There are two modes exhibiting strong responses in the loadbeam. The rocking mode at about 534 Hz is visible (Figure 14b), but it cannot be

estimated because the excitation energy is too small for the mode. The other modes are mainly related to the disks. There may be four modes among 1120-1180 Hz (Figure 14d), but only two modes could be estimated. Comparing with Table 2, the modes should be modes $(0,3)^2$. Two symmetric disks in the drive should have four (0,3) modes, and only two modes would be excited through the sliders. The sliders were located at the nodal line of the other two modes (see Figure 6), as the modes would not be excited by the sliders and suspension motions that were excited by the exciter on the arm. The actual disks are not perfectly symmetric, so the (0,3) modes show two higher peaks and two low peaks of the resonances in the measured FRFs.

Figure 15 shows the averaged FRFs measured in the other four bands. We can see that there are two kinds of modes. One has small damping, another exhibits much larger damping. The modes with small damping are grouped into four modes. These modes should correspond to the modes of the disks. Figure 16 shows that there is at least one mode that was not excited in the first experiment. This mode should be the mode that is mainly related to the arm, because the major difference between the two experiments is in the location of the excitation. Comparing with Figure 12, this mode should be the third bending mode of the arm-suspension. The first excitation point was occasionally located at the nodal line of the mode.

The slider's vibration in the lateral direction will result in off-track errors. Therefore, the response of the slider in the lateral direction was measured under the excitation in the Z direction. The measured FRFs are shown in Figure 17. Comparing Figure 17 c) with

Figure 16, we can see that the modes related to the arm, with frequency of about 4.4 kHz, would contribute a significant amount of off-track errors. The mode couples vertical motions with the lateral motion. Reviewing Figure 12, we can confirm that the mode should be the second torsional mode of the arm-suspension.

The modal frequencies and damping ratios of the modes can be estimated and are shown in Table 3, where we can see that the largest difference of the modal frequencies between the two experiments is less than 1.4%. The measured modal shapes are also very similar in the two experiments. The modal shapes measured in the second experiments are shown in Figure 18. The modal shapes of the grouped modes are very similar to each other, thus only one mode of the grouped modes is included in Figure 18. For convenience, the results of the two experiments were averaged and combined together, shown in Table 4, and they will be used as the experimental results in the following discussion.

Because only a small part of the drive was measured, it is difficult to exactly identify the modes based only on the measured mode shapes. The results shown in Table 2 and Figure 12 will be considered to identify the modes. We can classify the modes into three types. The first type is the strong suspension modes (S). There are no significant deformations of the components except the suspension assembly in the mode shapes of this type mode. From Figure 18, we can see that modes 11, 12, 24, 25, and 26 are strong suspension modes (modes 25, 26 are not shown in the figure), which are the first bending (S_{1B}), first torsional (S_{1T}) and second torsional (S_{2T}) modes, and flexure local modes (S_{FBO} flexure bending out of phase, S_{FBI} flexure bending in phase) of the assembly, respectively.

The second type of mode is the strong arm-suspension mode (AS), in which only the arm and suspension have significant deformations. Figure 18 shows modes 1, 2, 20-23 are strong arm-suspension modes. Modes 1 and 2 are the two first bending modes (AS_{1B}). The two first bending modes could come from more than one arm-suspension in the drive. It is surprising that their frequencies are so low. These are much lower than the frequency of the first bending mode of the suspension. As mentioned above, modes 20 and 21 should be the second torsional (AS_{2T}) and third bending (AS_{3B}) modes, respectively.

The third type is the coupled mode. The nomenclature with two parts is used to designate the mode shapes. The first part AS or S is used to identify the shape of the arm-suspension or suspension, and the second $DK_{(m,n)}$ is used to identify the shape of the disk. The modes were identified, and are shown in Table 4. The modal frequencies of modes 16-19 are close, so it cannot be determined which is mode (0, 6) or (1, 1). It is found that the mode shapes of the arm-suspension and suspension in the coupled modes are mainly dependent on their frequencies. If the frequencies of the coupled modes are close to the frequencies of the individual arm-suspension or suspension assembly, the mode shapes of the arm and/or suspension in the coupled modes will be similar to the corresponding shapes of the individual components. For example, the frequency of mode 3 is close to the first bending mode of the arm-suspension. The arm-suspension shows the first bending shape in mode 3. The frequency of mode 10 is close to the first bending mode of the suspension. The suspension has the first bending shape in mode 10.

From Table 4, we can see that the types 1 and 2 modes have much larger modal damping ratios than the coupled modes. The interface between the sliders and the disks may contribute much damping to the resonances. Comparing Table 4 with Figure 12, we can see that almost all modes of the individual arm-suspension are included in the modes of the drive as local modes, and their frequencies are very close to the ones of the individual components. That means the arm-suspension is a relatively independent component. The lower damping ratios of the coupled mode may imply that there are no relative motions between the sliders and the disks when the drive is vibrated in the coupled modes. If this is indeed true, the coupled modes would contribute little to the off-tracking errors.

6. DYNAMIC ANALYSIS OF THE DRIVE

6.1 FE Model of the Drive

To better understand the dynamic behavior of the drive, a simplified FE model of the drive was created by the Parametric Design Language of the ANSYS FE code, and is shown in Figure 19. Only one disk and two arm-suspensions with the same parameters are included in the model. The FE models of the disk shown in Figure 4 and the arm-suspension shown Figure 7 were defined in their local coordinate systems, and combined together. Then, the model of the arm-suspension was reflected with respect to the XY plane. The interfaces between each slider and disk were modeled by four coupled DOFs, that is, four nodes on the four corners of the slider were allowed to have no relative translational motions to four nodes on the disk (each of which is at the nearest location to the corresponding corners) in the axial direction of the disk, but are allowed have relative

motions in the remaining DOFs (two translational and three rotational DOFs). The entire model consists of about 130 design parameters, 3202 SHELL63, 24 SOLID45, and 3672 SOLID73 elements. The number of total active DOFs is 29662. The model was used to analyze the modal parameters of the drive and predict the properties when the disks were rotating. The sensitivity of the design parameters of the drive can be easily analyzed because the model was created by the Design Parametric Language.

6.2 Analyzed Modal Parameters of the Drive

The modes in the frequency band of 0-10 kHz were calculated by the subspace iteration method, and fifty-two modes were obtained. Besides the three type modes that were found in the experiments, an additional type mode was included in the analyzed modes. The additional type modes are the strong disk modes (DK), in which only the disk has significant deformations. All modal frequencies are listed in the Table 5 except for the strong disk and coupled modes with frequencies larger than 4.5 kHz. Some mode shapes are shown in Figure 20. Because the two arm-suspensions in the model are symmetry with the XY plane, each of the strong suspension and arm-suspension modes become two modes. One is the deformation of the suspensions or arm-suspensions in phase (I), and another is out of phase (O). Their frequencies are close to each other. Because of the symmetry of the disk, the mode (m, n) of the individual disk with one modal frequency and two orthogonal mode shapes (n>0) becomes two modes with close modal frequencies in the coupled system. One of the two modes is the strong disk mode, another is the coupled mode. Checking the mode shapes shown in Figure 20, we can see that only the coupled mode could be excited by the vibration of the arm-suspension because the sliders

are located at the peak line of this mode. The strong disk mode could not be excited because the sliders are located at the nodal line of that mode. So, the strong disk modes were not found in the experiments. The two larger peaks in Figure 14 d) should come from the two disks in the drive, and correspond to the coupled modes. The two smaller peaks should correspond to the strong disk modes of the two disks for the small asymmetry of the disks.

We cannot match each single mode between the experimental and analytical results because the frequencies of the modes in the grouped modes are too close, the measured region of the drive is too small, and only one disk is included in the FE model. For example, only one suspension was measured, thus the modes in phase and out of phase cannot be identified from the measured modes. Therefore, comparisons shown in Table 5 are made in the groups. Comparing the analyzed results with the experimental results, good correlation was achieved. Figure 20 shows the location of the sliders is near the nodal circle of mode (1, 0). Thus, this mode cannot be excited and estimated by the experiment.

6.3 Predicted Properties with Rotating Disks

The experiments and analysis had previously been made with the disks stationary. It is well known that the behavior of the drive will be changed when the disks in the drive are rotating. There are two effects of the rotating speed on the dynamic properties. One is the amplitude modulation that produces so-called forward and backward modes. Another is increasing stiffness for the prestress in the rotating disk. If mode (m, n) has modal

frequency ω_{nm} in the stationary state, when the disk is rotating, the observed modal frequency in the stationary coordinate system will be

$$\omega_{nm}^{F} = \omega_{nm} + n\Omega \tag{2}$$

$$\omega_{nm}^{B} = \omega_{nm} - n\Omega \tag{3}$$

where Ω is the rotation speed of the disk, ω_{nm}^{F}, ω_{nm}^{B} are the modal frequencies of the forward and backward modes of the (m, n) mode. The measured Ω of the drive is 544.75 rad/s (about 5202 RPM). The analyzed frequencies of the coupled modes (m, n) in Table 5 were used as ω_{nm} , and substituted into Eqs. (2) and (3). The predicted modal frequencies of the coupled modes of the drive with the rotating disks were obtained, and are shown in Table 6. At 5200 RPM, the split of the $AS_{1B}DK_{(0,1)}$ mode (606.43 Hz) results in 519.76 Hz for the backward mode and 693.10 Hz for the forward mode. The other coupled modes will have a similar split phenomena, depending on the number of the nodal diameters n.

To calculate the effect of the prestress, the modal frequency changes of the (m, n) mode for the prestressed effects, which are shown in Table 2, were added into the modal frequencies of the coupled mode corresponding to the (m, n) modes. The results were used as $\omega_{nm,}$ and then substituted into Eqs. (2) and (3). Finally, the predicted modal frequencies of the coupled modes of the drive with the prestressed effects when the disks are rotating were obtained, and are shown in Table 6. The modal frequencies increase about 10 Hz for each coupled mode due to the prestressed effects. Therefore, when the disks are rotating, the $AS_{1B}AK_{(0,1)}$ mode will have two frequencies. One is about 529.36

Hz (backward mode $AS_{1B}AK_{(0,1)}^{-}$), another is about 702.70 Hz. (forward mode $AS_{1B}AK_{(0,1)}^{+}$).

7. EXPERIMENTS OF THE DRIVE – DISKS ROTATING

7.1 Power Spectrum Measurement

Using the same drive and experimental setup, measurements of the vibration power spectrum and modal experiment were performed while the disks were rotating after the first experiment with stationary disks was finished. When the disks are rotating and the artificial excitation is not applied, the spindle motor and windage will excite the vibration of the components in the drive. The vibration displacements of the slider at point 62 and the suspension at point 6 (Figure 13) in the Z direction were measured in the frequency band of .5-10 kHz. The band was divided into four sub-regions: .5-1, 1-2.6, 2.6-5.1, and 5.1-10.1 kHz. The displacement output of the LDV was fed into the Analyzer, and the power spectra (PS) were computed with the Hanning window and thirty averages. The curves have μm^2 units in RMS. The measured PS are shown in Figure 21.

From Figure 21, we can see that there are two types of vibration in the drive. The first one is excited by the spindle motor, which shows many discrete peaks in the curves. The second is the structural resonance, which exhibits some peaks with a wider band. Using Tables 5 and 6, we can identify each peak that represents the structural resonance. Most of the coupled modes (i.e., 1550, 2250, 2450 Hz) show two peaks because the drive has two disks. When the disks are rotating, the excitation is similar to that where the arm-suspensions were excited by artificial excitations at the slider. The figure shows that all

modes of the suspension and arm-suspension were excited. To better understand the properties of the structural resonances, a modal experiment was performed when the disks were rotating.

7.2 Modal Experiment of the Drive with Rotating Disks

The geometric model used in the experiment is shown in Figure 22. Points 1-5 are located on the tip of the actuator arm. There are seven points (51-57) on the flexure and two points (61, 62) on the slider. The excitation point was the same as in the first modal experiment. For the rotating disks experiment, the disks were not included in the geometric model. Considering the measured PS, the frequency range of 0-10 kHz was divided into five frequency bands: 410-1660, 1700-3262, 3200-4762, 4600-6200, and 6100-10100 Hz. The periodic chirp signal was used in the excitation because there should be no Coulomb damping between the sliders and the disks with the air bearing existing between them. When the power is turned on, the disks start rotating, and the sliders are automatically set at the outer diameter. The location of the sliders is automatically changed after about 10 minutes. For consistency of the results, each FRF should be measured before the location is changed. If the location was changed, the power was turned off, and then turned on again. For each band, forty FRFs were measured in the Z direction under the control of the software. Figure 23 shows the measured FRFs averaged in some chosen bands. The modal parameters were obtained by curve fitting and the mode sorting. The measured modal frequencies, damping ratios and mode shape identifications are shown in Table 7. Some measured mode shapes are shown in Figure 24 as examples.

The modal experimental results of the drive with rotating disks show that: ❶ The predicted frequencies by FE analysis are very close to the measured values. ❷ The assignment of the modal frequencies of the drive is suitable. No modal frequencies of the coupled modes are close to the ones of the suspension and the arm-suspension in the lower frequency band, otherwise resonances of the arm and/or suspension would be induced when disks are rotating. ❸ Most of the modal damping ratios are smaller than the ones measured with the disks in the stationary state. That is because there is no Coulomb damping in the interfaces between the sliders and the disks, and there were some excitations that were not measured. ❹ Comparing the mode shapes with the ones measured in the stationary state, there are some small differences in the shapes of the arm and/or suspension of the coupled modes. For example, when the disks are rotating, the backward mode (536.26 Hz) of mode (0, 2) is coupled with the cantilever bending mode of the arm-suspension. The forward mode (870.21 Hz) is coupled with the cantilever bending mode of the suspension. ❺ When the disks are rotating, there might be no strong disk modes because the mode (m, n) of the individual disk with one frequency and two orthogonal mode shapes becomes the forward and backward modes, which will be coupled with the arm-suspension. ❻ When the disks are rotating, the accuracy of the measured modal parameters of the coupled mode is relatively low because the artificial excitation level is not large enough compared to the other excitations. Some modes can not even be estimated, or the accuracy of the estimated damping ratios and mode shapes are very poor. For example, Figure 23 shows that there are two modes in the region of 3300 Hz , but we can only estimate one of them.

After the second experiment with stationary disks was finished, we attempted to perform the second experiment with rotating disks. However, the drive crashed when the tenth FRF was being measured. The cause might be the contamination since the disks were exposed in the ambient. Or it might be the artificial excitation that destroyed the air bearing, because a higher excitation level was applied to try to obtain more accurate results. It seems that it would be impossible to accurately measure the damping ratios and shapes of the coupled modes when the disks are rotating.

7.3 Vibration of the Slider in the Lateral Direction.

The off-track error is a well-known concern in the disk drive industry. To better understand which modes will contribute most to this error, the power spectrum of the slider's vibration in the lateral direction was measured when the disks were rotating and the artificial excitation was not applied. The state of the drive is almost the same as in the practical operating condition. First, the velocity PS in the frequency of 0-10 kHz was measured, and is shown in Figure 25. The figure shows that there are two strong vibration bands of many discrete peaks. The first band is between 4.5 kHz and 5.5 kHz, and the second band is between 7.2 kHz and 8.2 kHz. In order to learn more details of the vibration, a zoom analysis was performed. The PS in the frequency bands of .5-1 kHz, 1-2.6 kHz, 2.6-5.1 kHz and 5.1-10.1 kHz were measured, and are also shown in Figure 25. Based on the analytical and experimental results that were obtained, from Figure 25, we can state that: ❶ The first strong vibration band is mainly related to the second torsional mode and the first sway mode of the arm-suspension, and the strong vibration in the second band is the response of the second sway mode of the arm-suspension. Therefore,

the three modes contribute a significant amount of the lateral vibration of the slider. ❷ The bending modes of the suspension and/or arm (i.e., AS_{1B}, S_{1B}) contribute a small amount to the lateral vibration. The contribution of the second torsional mode of the suspension (S_{2T}) is larger than that of the first torsional mode (S_{1T}). ❸ The coupled modes also contribute to the lateral vibration. The relative vibration between the sliders and the disks will be much smaller because they are coupled to each other. As mentioned in McAllister (1996), the vibration from the coupled modes will be increased with the disk rotation speed.

8. SUMMARY

The dynamic behavior of a commercially available hard disk drive was investigated by experiments and FE analysis. The electromechanical components in the drive mainly consist of two 95 mm disks, three actuator arms, and four suspension assemblies with 50% sliders. The components were first studied. Then modal experiment was performed in the non-operation state of the drive. A simplified FE model of the drive, which included one disk, two actuator arms, and two suspension assemblies, was constructed. Using the FE model, the properties were predicted when the disks are rotating. Finally, a modal experiment of the drive with rotating disks was performed, and the power spectra of the vibration of the drive were measured. Good correlation between experiments and analysis was achieved. Some key observation of this work are:

1. An experimental system for modal experiment and vibration measurement of the drive was setup. The results show the system is robust for the drive experiments, although a higher excitation level is strongly recommended.

2. A relatively simple finite element model is capable of accurately modeling the drive. The dynamic properties of the drive in the non-operating and operating state can conveniently be predicted. The sensitivity of the design parameters can be easily analyzed because the model is created by the Design Parametric Language.

3. Because the drive is very complicated, to obtain accurate and reliable FE model of the drive, the FE model of the each component should be preliminarily created and individually validated by experiment. The results of component analysis are very helpful for understanding the properties of the entire drive.

4. The drive with stationary disks exhibits quite complicated dynamic properties. There are four types of modes: strong suspension modes, strong arm-suspension modes, strong disk modes, and coupled mode. All modes of the individual arm-suspension are included in the entire drive as local modes, and have larger modal damping ratios than other modes. All coupled modes correspond to the modes of the individual disks, and have smaller modal damping ratios. The shapes of the suspension and/or arm in the coupled modes are dependent on the modal frequencies of the modes.

5. The actuator arm plays a very important role in the dynamic properties of the drive. The arm induces a bending mode with frequency (555 Hz) much lower than that of the

first bending mode (2077 Hz) of the suspension, and it also contributes one additional torsional mode (4300 Hz) and two sway modes (5300 Hz and 7400 Hz).

6. Comparing the case of the rotating disks with the case of the stationary disks, there are no obvious changes in the strong suspension and arm-suspension modes. There are no strong disk modes, and each coupled mode is split into two modes - the forward and backward modes.

7. The measured power spectra of the slider's vibration in the lateral direction show that the second torsional and the first two sway modes of the arm-suspension will contribute a significant amount of the lateral vibration of the slider, and in turn result in off-track errors. The other modes give a much smaller amount of the off-track vibration.

ACKNOWLEDGMENTS

This study is supported by the Computer Mechanics Laboratory at the University of California at Berkeley. QHZ also acknowledges the support of the Chinese National Education Committee. We would like to thank Western Digital Company (Raju Ananth) for providing the test drives.

REFERENCES

Frees, G. M, 1995, “Disk Drive Spindle Dynamics - Analysis and Measurement”, ASME, Advances in Information Storage Systems, Vol. 6, pp. 237-262.

Ku, C. P. R., 1996, “Dynamic Characteristics of Hard Disk Drive Spindle Motors - Comparison Between Ball Bearings and Hydrodynamics Bearing”, ASME, Journal of Tribology, Vol. 118, No. 2, pp. 402-406.

McAllister, J. S., 1996, “The Effect of Platter Resonances on Track Misregistration in Disk Drives”, S/V Sound and Vibration, Jan., 1996, pp. 24-28.

Radwan, H. R. and Whaley R., 1993, “Servo-Structural Interaction in Disk Drives Using Finite Element Analysis”, ASME, Advances in Information Storage Systems, Vol. 3, pp. 101-118.

Wilson, C. J. and Bogy, D. B., 1993, “Experimental Modal Analysis of a Miniaturized Suspension/Disk Systems", CML report No. 93-009, Computer Mechanics Lab, Dept. of Mechanical Engineering, Univ. of California at Berkeley.

Wilson, C. J. and Bogy, D. B., 1994, “Experimental Modal Analysis of a Suspension Assembly Loaded on a Rotating Disk", ASME, Journal of Vibration and Acoustics, Vol. 116, No. 1, pp. 85-92.

Wilson, C. J. and Bogy, D. B., 1996, "An Experimental Modal Analysis Technique For Miniature Structures", Transactions of the ASME, Journal of Vibration and Acoustics, Vol. 118, No. 1, pp. 1-9.

Yoshida, T., Hirai H., et al., 1995, “Vibration Reduction of a Small Magnetic Disk Drive Using a Nonreacting, Twin-Drive Actuator”, ASME, Advances in Information Storage Systems, Vol. 5, pp. 289-300.

Zeng, Q. H. and Bogy, D. B., 1996a, “Experimental Modal Analysis Technique, System and Application for Miniature Structures”, CML report No. 96-011, Computer Mechanics Lab., Dept. of Mechanical Engineering, Univ. of California at Berkeley, May, 1996.

Zeng, Q. H. and Bogy, D. B., 1996b, “Modal Dynamics Experiment and Analysis of a Suspension Assembly Used in Hard Disk Drives”, CML report No. 96-013, Computer Mechanics Lab., Dept. of Mechanical Engineering, Univ. of California at Berkeley, June, 1996.

No	**Measured**	Initial FE Model		Updated FE Model		Mode
	Freq.(Hz)	Freq.(Hz)	Diff.(%)	Freq.(Hz)	Diff.(%)	Shape
1	**422.5**	436.5	3.31	427.4	1.16	$(0, 2)^2$
2	**740.6**	739.2	-0.19	723.5	-2.31	(0, 0)
3	**1049**	1077	2.67	1054	0.48	$(0, 3)^2$
4	**1643**	1677	2.07	1632	-0.67	$(1, 1)^2$
5	**1862**	1908	2.47	1867	0.27	$(0, 4)^2$
6	**2864**	2935	2.48	2873	0.31	$(0, 5)^2$
7	**2932**	2966	1.16	2904	-0.95	$(1, 2)^2$
8	**4057**	4114	1.4	4020	-0.91	(2, 0)
9	**4085**	4160	1.84	4072	-0.32	$(0, 6)^2$

Table 1 Measured and analyzed modal frequencies of the disk in its free state
Mode shape $(m, n)^r$, where, m is the number of nodal circles,
n is the number of nodal diameters,
r is the number of the mode

No	**Measured**	FE Model		Prestressed FE Model		Mode
	Freq.(Hz)	Freq.(Hz)	Diff.(%)	Freq.(Hz)	Change(Hz)	Shape
1	**603.5**	604.3	0.13	613.9	9.6	$(0, 1)^2$
2	**616.5**	613.1	-0.55	621.0	7.9	(1, 0)
3	**699.5**	714.6	2.16	726.9	12.3	$(0, 2)^2$
4	**1153**	1153	0.0	1164	11	$(0, 3)^2$
5	**1900**	1899	-0.05	1909	10	$(0, 4)^2$
6	**2890**	2886	-0.14	2896	10	$(0, 5)^2$
7		3917		3926	9	(2, 0)
8	**4058**	4084	0.64	4093	9	$(0, 6)^2$
9	**4073**	4085	0.29	4094	9	$(2, 1)^2$

Table 2 Measured and analyzed modal frequencies of the disk in its clamped state
Mode shape $(m, n)^r$, where, m is the number of nodal circles,
n is the number of nodal diameters,
r is the number of the mode

No	Modal Frequency (Hz)			Damping Ratios(%)	
	First Experiment	Second Experiment	Difference (%)	First Experiment	Second Experiment
1	***555.24***	***559.89***	***0.84***	***.99***	***1.02***
2	***570.26***	***572.59***	***0.41***	***.37***	***.25***
3	606.80	602.69	- 0.68	.22	.043
4	616.49	618.05	0.25	.083	.064
5	685.22	694.04	1.29	.12	.097
6	709.23	703.61	- 0.79	.12	.13
7	1129.3	1131.5	0.19	.064	.066
8	1151.1			.089	
9	1862.0	1866.0	0.21	.070	.059
10	1876.2	1879.6	0.18	.061	.064
11	**2059.7**	**2077.2**	**0.85**	**.35**	**.28**
12	**2765.5**	**2802.7**	**1.35**	**.55**	**.71**
13	2868.0	2872.2	0.15	.033	.031
14	2880.1	2883.4	0.11	.030	.032
15	2892.2	2905.4	0.46	.034	.068
16	4050.9	4056.7	0.14	.032	.030
17	4064.4	4071.5	0.17	.035	.046
18	4082.5	4087.3	0.12	.034	.029
19		4104.2			.054
20		***4461.8***			***.43***
21	***4526.7***	***4522.0***	***- 0.10***	***.30***	***.51***
22	***4945.6***	***4973.4***	***0.56***	***.58***	***.41***
23	***5361.2***	***5364.3***	***0.06***	***.64***	***.50***
24	**8120.1**	**8200.9**	**1.00**	**.24**	**.36**
25	**9654.3**	**9684.1**	**0.31**	**.21**	**.25**
26	**9816.8**	**9856.2**	**0.40**	**.29**	**.22**

Table 3 Modal frequencies and damping ratios of the drive with stationary disks -- Comparison of the two experiments

No	Modal Frequency	Damping Ratio(%)	Mode Shape			
			Suspension	Arm-Susp.	Disk	Nomenclature
1	***557.57***	***1.01***		***1st Bending***		***AS_{1B}***
2	***571.43***	***.31***		***1st Bending***		***AS_{1B}***
3	604.75	.13		1st Bending	(0,1)	$AS_{1B}DK_{(0,1)}$
4	617.27	.074		1st Bending	(0,0)	$AS_{1B}DK_{(0,0)}$
5	689.63	.11		1st Bending	(0,2)	$AS_{1B}DK_{(0,2)}$
6	706.43	.13		1st Bending	(0,2)	$AS_{1B}DK_{(0,2)}$
7	1130.4	.065		**C**antilever	(0,3)	$AS_{1C}DK_{(0,3)}$
8	1151.1	.089		Cantilever	(0,3)	$AS_{1C}DK_{(0,3)}$
9	1864.0	.065	1B & **C**antil.		(0,4)	$S_{BC}DK_{(0,4)}$
10	1877.9	.063	1B & Cantil.		(0,4)	$S_{BC}DK_{(0,4)}$
11	**2068.5**	**.32**	**1st Bending**			**S_{1B}**
12	**2784.1**	**.63**	**1st Bending**			**S_{1T}**
13	2870.1	.032	**B&C&T**ors.		(0,5)	$S_{BCT}DK_{(0,5)}$
14	2881.5	.031	**B&C&T**ors.		(0,5)	$S_{BCT}DK_{(0,5)}$
15	2898.8	.051	**B&C&T**ors.		(0,5)	$S_{BCT}DK_{(0,5)}$
16	4053.8	.031		Bend.&Tors.	(0,6)	$AS_{BT}DK_{(0,6)}$
17	4068.0	.041		Bend.&Tors.	(0,6)	$AS_{BT}DK_{(0,6)}$
18	4084.9	.032		Bend.&Tors.	(1,1)	$AS_{BT}DK_{(1,1)}$
19	4104.2	.054		Bend.&Tors.	(1,1)	$AS_{BT}DK_{(1,1)}$
20	***4461.8***	***.43***		***2nd Torsion***		***AS_{2T}***
21	***4523.2***	***.41***		***3rd Bending***		***AS_{3B}***
22	***4959.5***	***.50***		***(Bending?)***		***($AS_{?B}$)***
23	***5362.8***	***.57***		***(1st Sway?)***		***(AS_{1SW})***
24	**8160.5**	**.30**	**2nd Torsion**			**S_{2T}**
25	**9669.2**	**.23**	**Flex. Bend**			**S_{FB}**
26	**9836.5**	**.25**	**Flex. Bend**			**S_{FB}**

Table 4 Measured modal parameters of the drive with stationary disks

No	Modal Frequency		Mode Shape	
	FE Analysis	Experiment	Nomenclat.	Description
1	591.40	557.57	AS_{1B}^{I}	**1**st **B**ending of **A**rm-**S**usp. **I**n phase
2	597.66	571.43	AS_{1B}^{O}	**1**st **B**ending of **A**-**S**. **O**ut of phase
3	604.76	604.75	$DK_{(0,1)}$	**D**is**k (0,1)** only
4	606.43		$AS_{1B}^{I}DK_{(0,1)}$	**D**is**k (0,1)** coupled with **1B** of **A**-**S**
5	613.28	617.27	$AS_{1B}^{I}DK_{(0,0)}$	**D**is**k (0,0)** coupled with **1B** of **A**-**S**
6	712.31	689.63 706.43	$AS_{1B}^{I}DK_{(0,2)}$	**D**is**k (0,2)** coupled with **1B** of **A**-**S**
7	716.59		$DK_{(0,2)}$	**D**is**k (0,2)** only
8	1147.3	1130.4 1151.1	$S_{1C}^{I}DK_{(0,3)}$	**D**is**k (0,3)** with **C**antilever bend of **S.**
9	1156.2		$DK_{(0,3)}$	**D**is**k (0,3)** only
10	1884.2	1864.0 1877.9	$S_{BC}^{I}DK_{(0,4)}$	**D**is**k (0,4)** with **B.** & **C**antil. of **S**
11	1904.0		$DK_{(0,4)}$	**D**is**k (0,4)** only
12	2239.0	2068.5	S_{1B}^{O}	**1**st **B**ending of **S**. **O**ut of phase
13	2252.0		S_{1B}^{I}	**1**st **B**ending of **S**. **I**n phase
14	2721.4	2784.1	S_{1T}^{I}	**1**st **T**orsion of **S**. **I**n phase
15	2721.4		S_{1T}^{O}	**1**st **T**orsion of **S**. **O**ut of phase
16	2882.8	2870.1 2881.5	$S_{BCT}^{I}DK_{(0,5)}$	**D**is**k (0,5)** with **B.**& **C.**& **T.** of **A**-**S**
17	2893.1	2898.8	$DK_{(0,5)}$	**D**is**k (0,5)** only
18	3915.4		$AS_{3B}^{I}DK_{(1,0)}$	**D**is**k (1,0)** with **B**end of **A**-**S**
19	4014.9	4461.8	AS_{2T}^{I}	**2**nd **T**orsion of **A**rm-**S**usp. **I**n phase
20	4015.7		AS_{2T}^{O}	**2**nd **T**orsion of **A**-**S**. **O**ut of phase

(Continued in next page)

Table 5 Analyzed and measured modal parameters of the drive with stationary disks

No	Modal Frequency		Mode Shapes	
	FE Analysis	Experiment	Notation	Description
21	4067.6	4053.8	$AS_{BT}{}^{I}DK_{(0,6)}$	**D**is**k (0,6)** with **B&T** of **A-S**
22	4084.3	4068.0	$DK_{(1,1)}$	**D**is**k (1,1)** only
23	4084.4	4084.9	$DK_{(1,1)}$	**D**is**k (1,1)** only
24	4094.2	4104.2	$DK_{(0,6)}$	**D**is**k (0,6)** only
25	4538.8	4523.2	$AS_{3B}{}^{I}$	**3rd B**ending of **A**rm-**S**uspension
26	4539.1	(4959.5 ?)	$AS_{3B}{}^{O}$	**3rd B**ending of **A**rm-**S**uspension
27	5386.3	(5362.8 ?)	$AS_{1SW}{}^{O}$	**1**st **Sw**ay of **A**rm-**S**uspension
28	5386.4		$AS_{1SW}{}^{I}$	**1**st **Sw**ay of **A**rm-**S**uspension
29	6353.2		$S_{2B}{}^{O}$	**2**nd **B**ending of **S**. **O**ut of phase
30	6367.1		$S_{2B}{}^{I}$	**2**nd **B**ending of **S**uspension in phase
31	7386.0		$AS_{2SW}{}^{I}$	**2**nd **Sw**ay of **A**rm-**S**uspension
32	7386.0		$AS_{2SW}{}^{O}$	**2**nd **Sw**ay of **A**rm-**S**uspension
33	8010.6	8160.5	$S_{2T}{}^{I}$	**2**nd **T**orsion of **S**uspension **I**n phase
34	8010.6		$S_{2T}{}^{O}$	**2**nd **T**orsion of **S**. **O**ut of phase
35	9584.7	9669.2	$S_{FBO}{}^{I}$	**F**lexure **B**end (**O**ut of phase) **O**ut of phase and **I**n phase
36	9584.8		$S_{FBO}{}^{O}$	
37	9864.8	9836.5	$S_{FBI}{}^{O}$	**F**lexure **B**end (**I**n phase) **O**ut of phase and **I**n phase
38	9871.9		$S_{FBI}{}^{I}$	

Table 5 (Continued) Analyzed and measured modal parameters of the drive with stationary disks

No	Disk Stationary	Predicted Modal Frequency while Disk Is Rotating				Mode Shape of the Disk
		Without Prestress		With Prestress		
		Backward	Forward	Backward	Forward	
1	606.43	519.76	693.10	529.36	702.70	(0, 1)
2	613.28	613.28		621.18		(0, 0)
3	712.31	538.98	885.64	551.28	897.94	(0, 2)
4	1147.3	887.30	1407.3	898.30	1418.3	(0, 3)
5	1884.2	1537.5	2230.9	1547.5	2240.9	(0, 4)
6	2882.8	2449.5	3316.1	2459.5	3326.1	(0, 5)
7	3915.4	3915.4		3924.4		(1, 0)
8	4067.6	3547.6	4587.6	3556.6	4596.6	(0, 6)
9	4084.3	3997.6	4171.0	4006.6	4180.0	(1, 1)

Table 6 Predicted modal frequencies of the coupled modes of the drive with rotating disks

No	FE Analysis	Experiment		Mode Shape
	Frequency (Hz)	Frequency (Hz)	Damping Ratio (%)	
1	529.36	521.73	.050	$AS_{1C}DK_{(0,1)}^{-}$
2	551.28	536.26	.023	$AS_{1C}DK_{(0,2)}^{-}$
3	591.40	555.30	1.09	AS_{1B}^{I}
4	597.66	568.79	.30	AS_{1B}^{O}
5	621.18	619.47	.030	$AS_{1B}DK_{(0,0)}$
6	702.70	690.68	.0056	$AS_{1B}DK_{(0,1)}^{+}$
7	897.94	870.21	.11	$S_{1C}DK_{(0,2)}^{+}$
8	898.30	881.25 886.76	.083 .062	$S_{1C}DK_{(0,3)}^{-}$
9	1418.3	1398.9 1410.5	.050 .013	$S_{1C}DK_{(0,3)}^{+}$
10	1547.5	1546.9 1555.2	.033 .017	$S_{1C}DK_{(0,4)}^{-}$
11	2239.0	2034.2	.086	S_{1B}^{O}
12	2252.0			S_{1B}^{I}
13	2240.9	2240.8 2254.1	.023 .0067	$S_{1B}DK_{(0,4)}^{+}$
14	2459.5	2450.1 2461.7	.013 .040	$S_{1B}DK_{(0,5)}^{-}$
15	2721.4	2723.7	.18	S_{1T}^{I}
16	2721.4			S_{1T}^{O}

(Continued in next page)

Table 7 Analyzed and measured modal frequencies of the drive with rotating disks

No	FE Analysis	Experiment		Mode Shape
	Frequency (Hz)	Frequency (Hz)	Damping Ratio (%)	
17	3326.1	3306.6	.0099	$AS_{??}DK_{(0,5)}^{+}$
18	3556.6	3550.8 3563.5	.0021 .0027	$AS_{??}DK_{(0,6)}^{-}$
19	3924.4			$AS_{3BT}DK_{(1,0)}$
20	4006.6			$AS_{??}DK_{(1,1)}^{-}$
21	4014.9			AS_{2T}^{I}
22	4015.7			AS_{2T}^{O}
23	4180.0			$AS_{??}DK_{(1,1)}^{+}$
24	4538.8	4394.5	.12	AS_{3B}^{I}
25	4539.1	(4774.8)	(.037)	AS_{3B}^{O}
26	4595.6	4580.3 4596.0	.056 .037	$AS_{1B}DK_{(0,6)}^{+}$
27	5386.3	(5375.5)	(.024)	AS_{1SW}^{I}
28	5386.4			AS_{1SW}^{O}
29	6353.2			S_{2B}^{I}
30	6367.1			S_{2B}^{O}
31	7386.0			AS_{2SW}^{I}
32	7386.0			AS_{2SW}^{O}
33	8010.6	8077.8	.20	S_{2T}^{I}
34	8010.6			S_{2T}^{O}
35	9584.7	9493.4	.034	S_{FBO}^{I}
36	9584.8			S_{FBO}^{O}
37	9864.8	9600.0	.050	S_{FBI}^{O}
38	9871.9			S_{FBI}^{I}

Table 7(Continued) Analyzed and measured modal frequencies of the drive with rotating disks

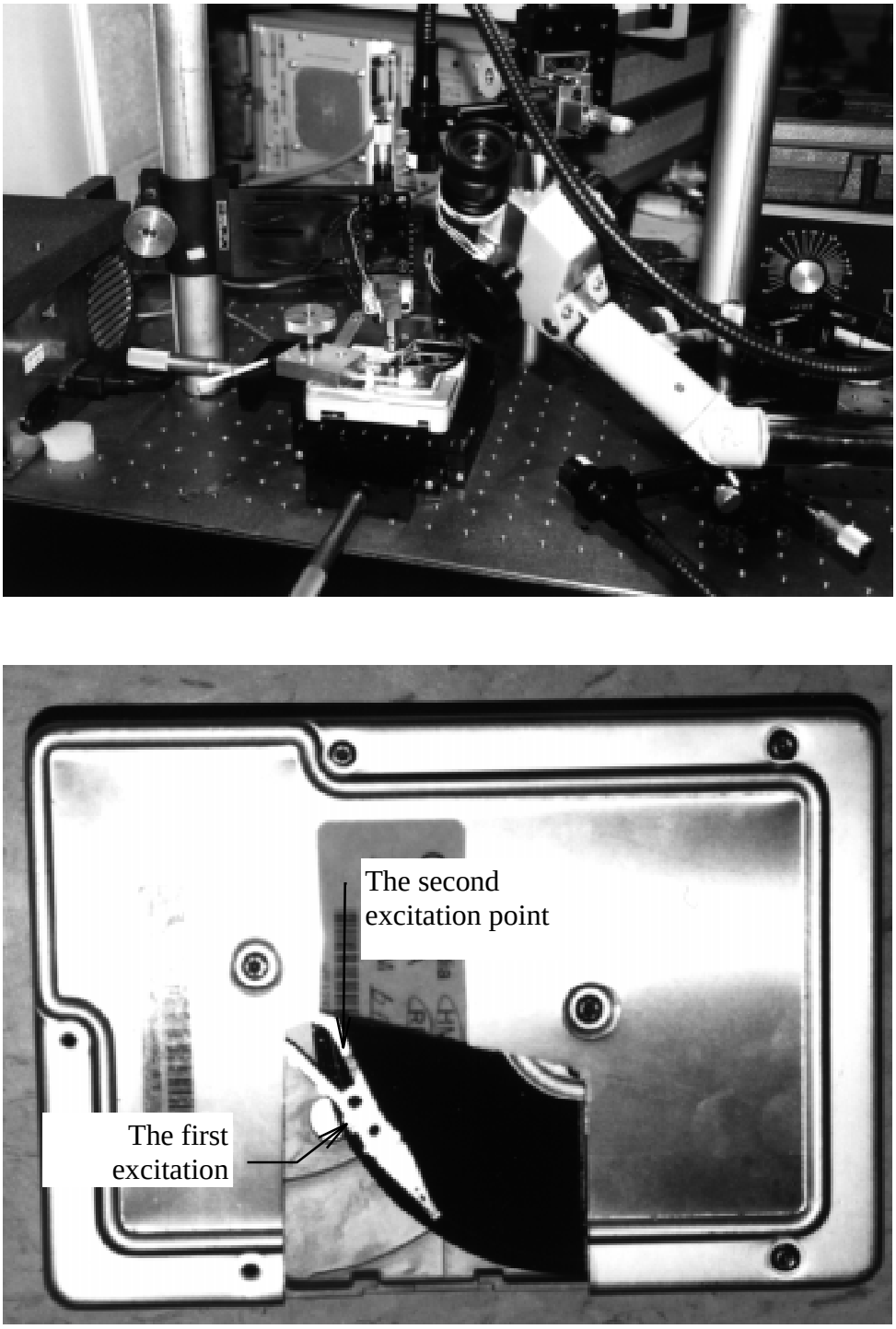

Figure 1 The experimental setup and the hard disk drive used in the research

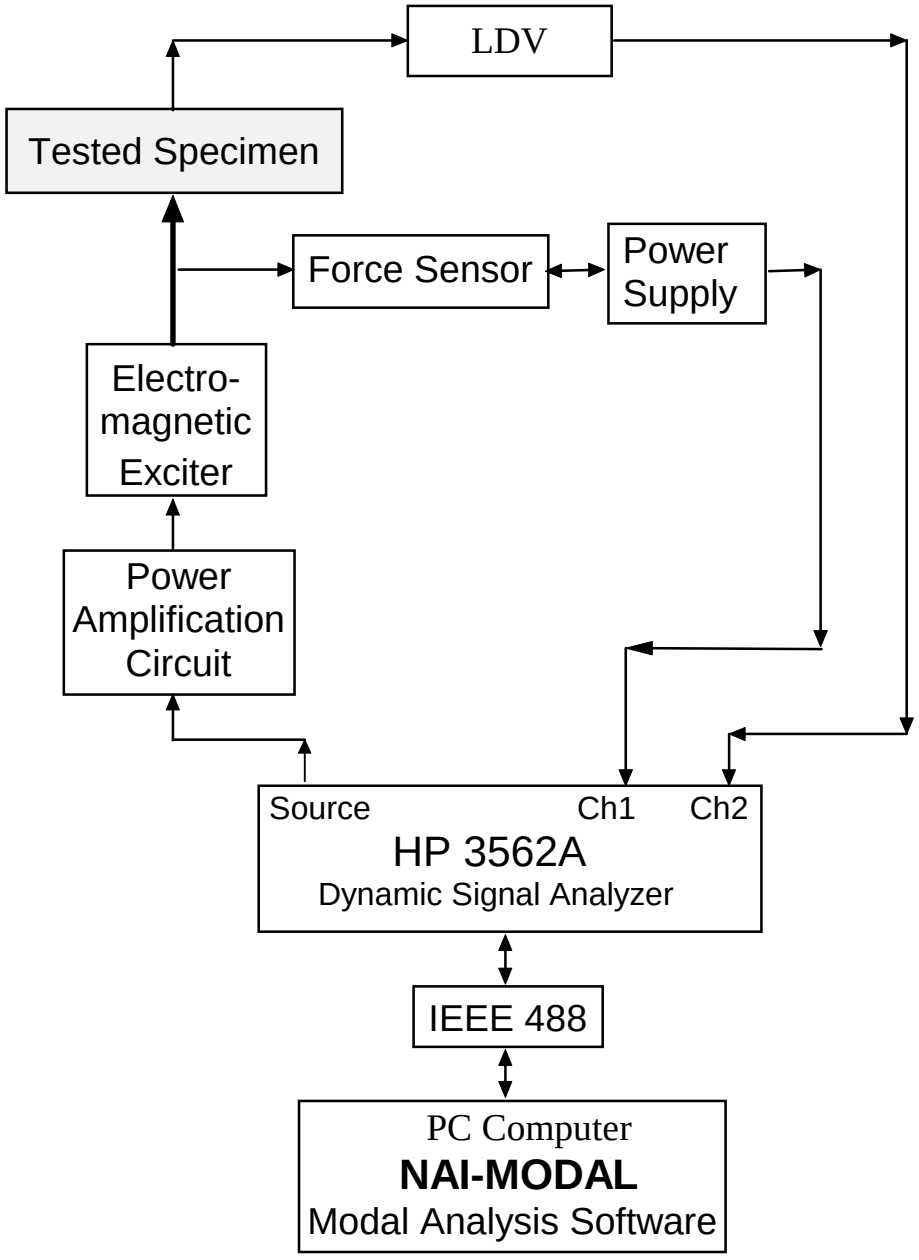

Figure 2 Schematic of the experimental system

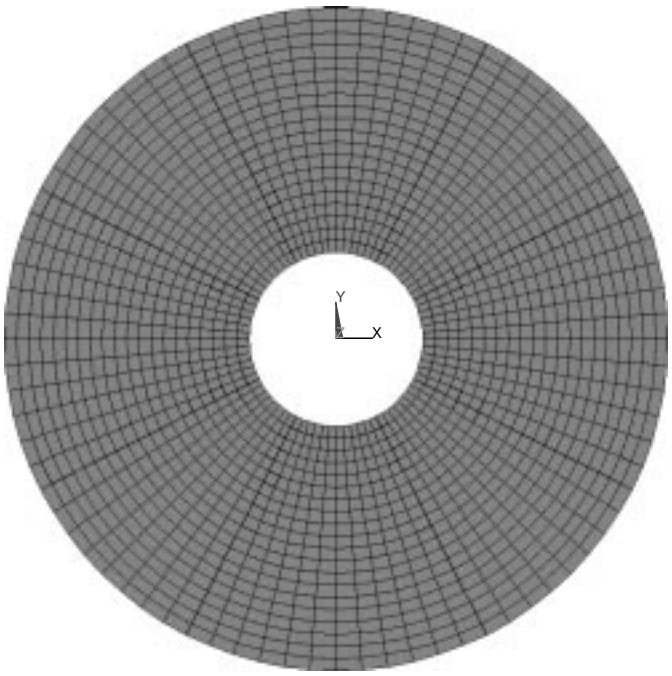

Figure 3 An FE model of the disk in its free state

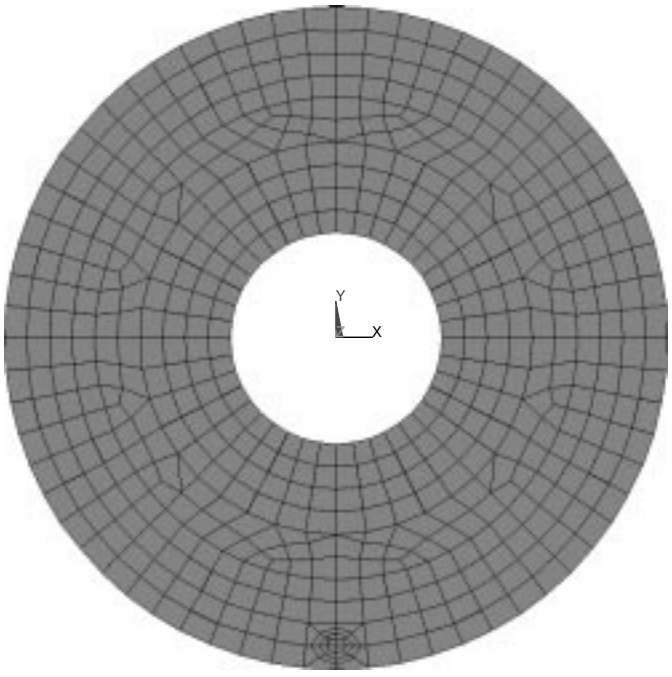

Figure 4 An FE Model of the disk clamped at the inner diameter

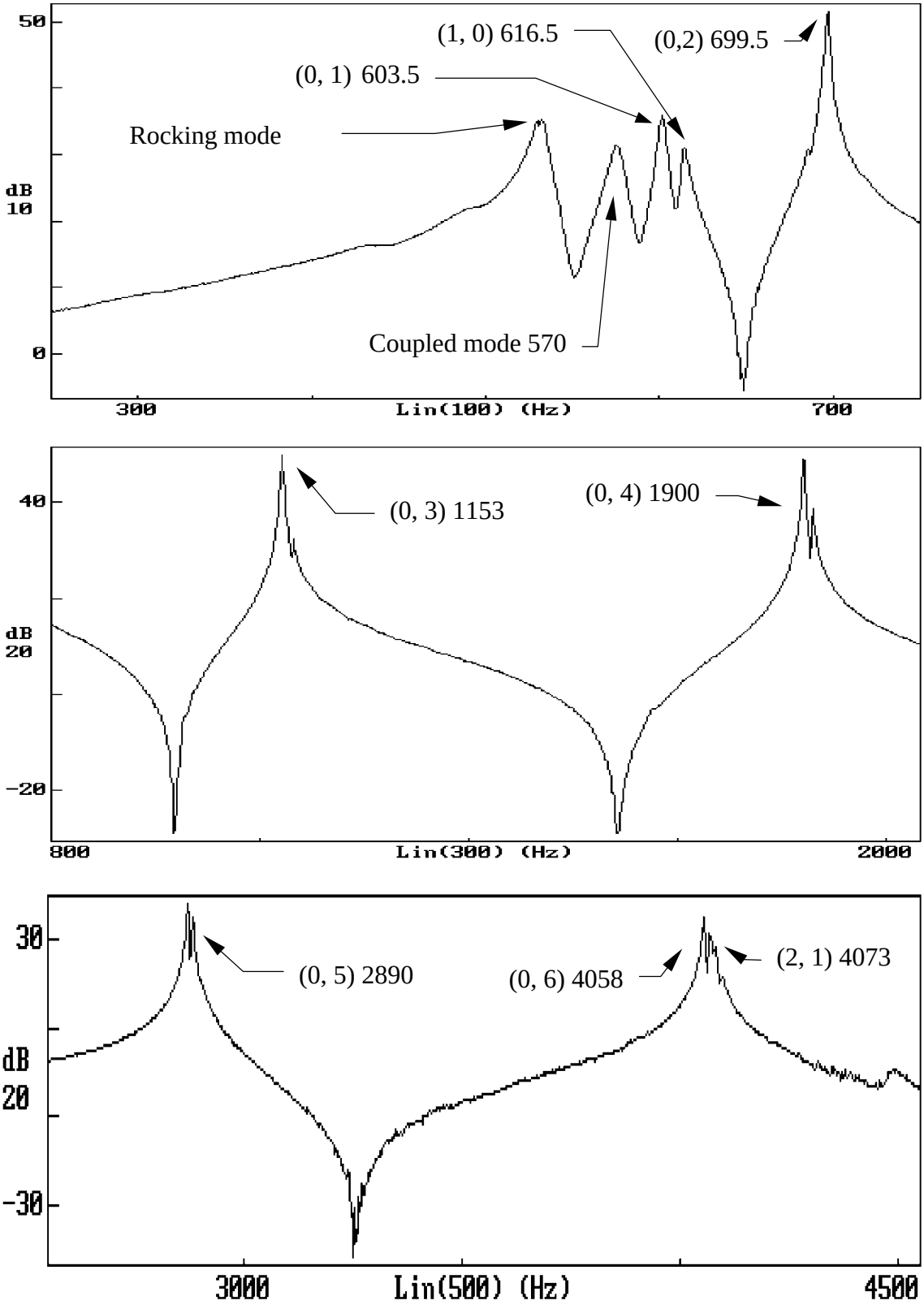

Figure 5 Measured FRFs of the drive
(Measuring and impacting the upper disk at the outer diameter)

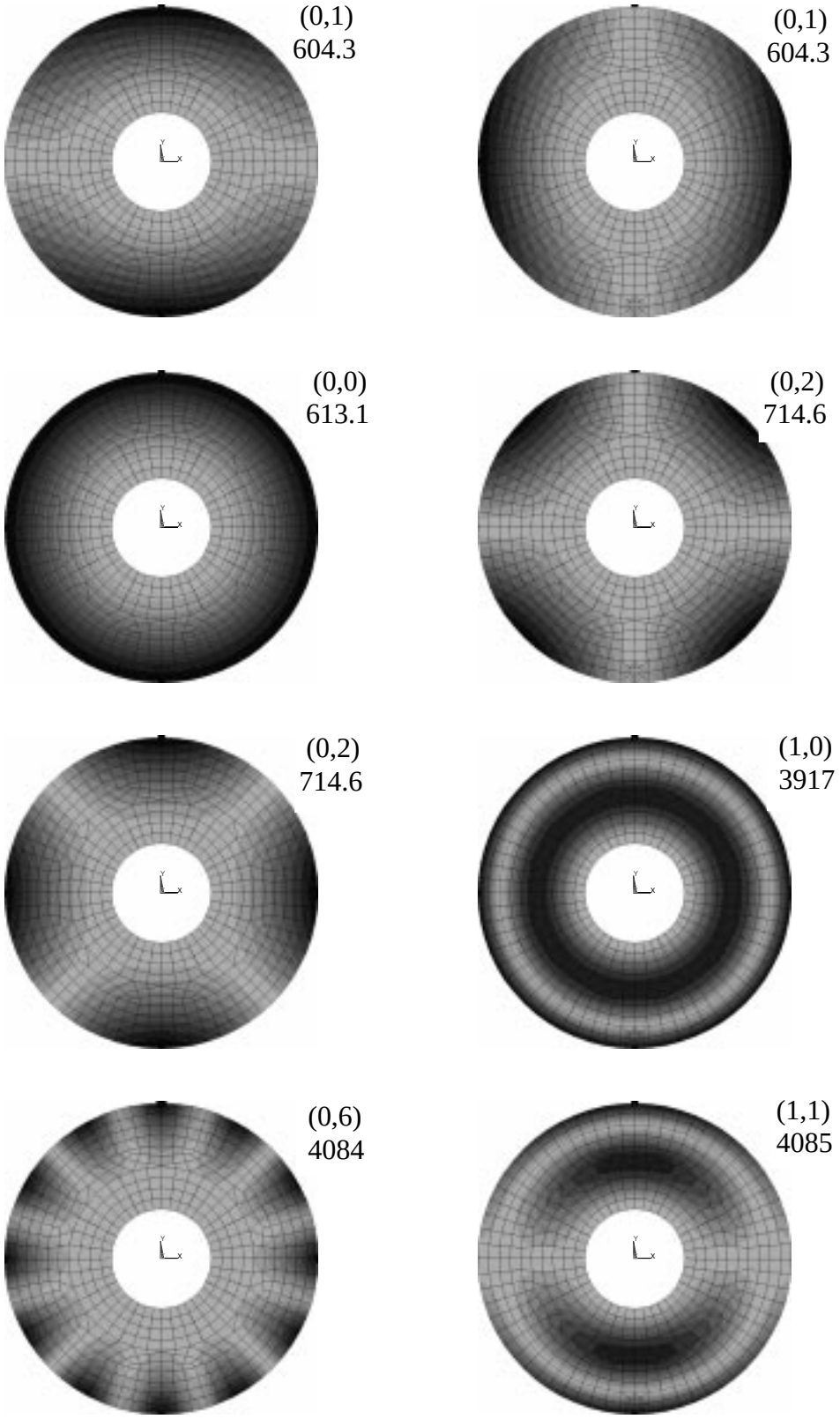

Figure 6 Analyzed mode shapes of the disk clamped at the inner diameter

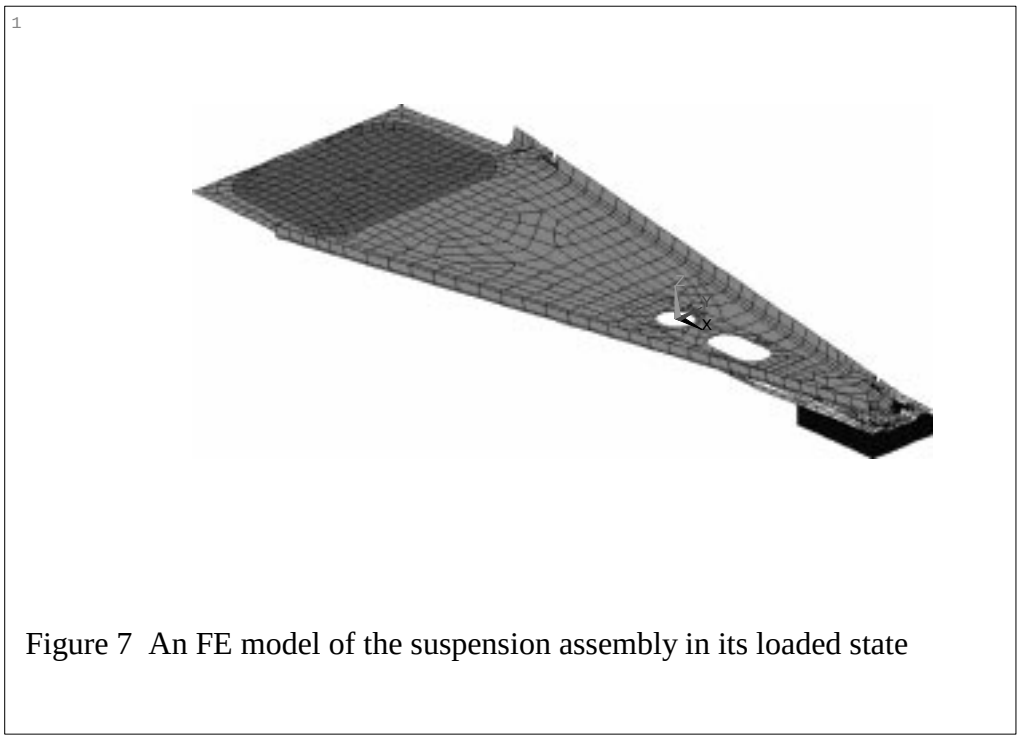

Figure 7 An FE model of the suspension assembly in its loaded state

Figure 8 Analyzed modal parameters of the suspension assembly in its loaded state

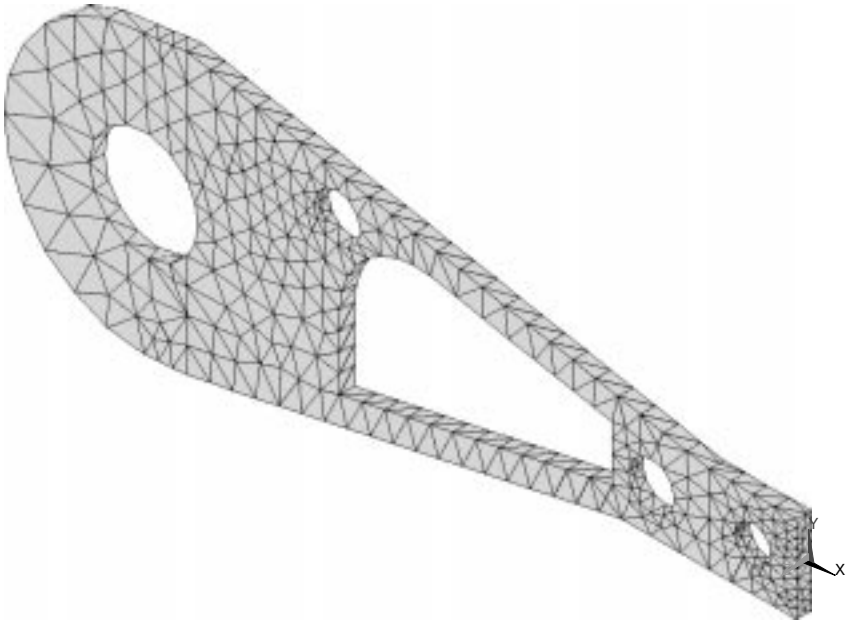

Figure 9 An FE model of the actuator arm

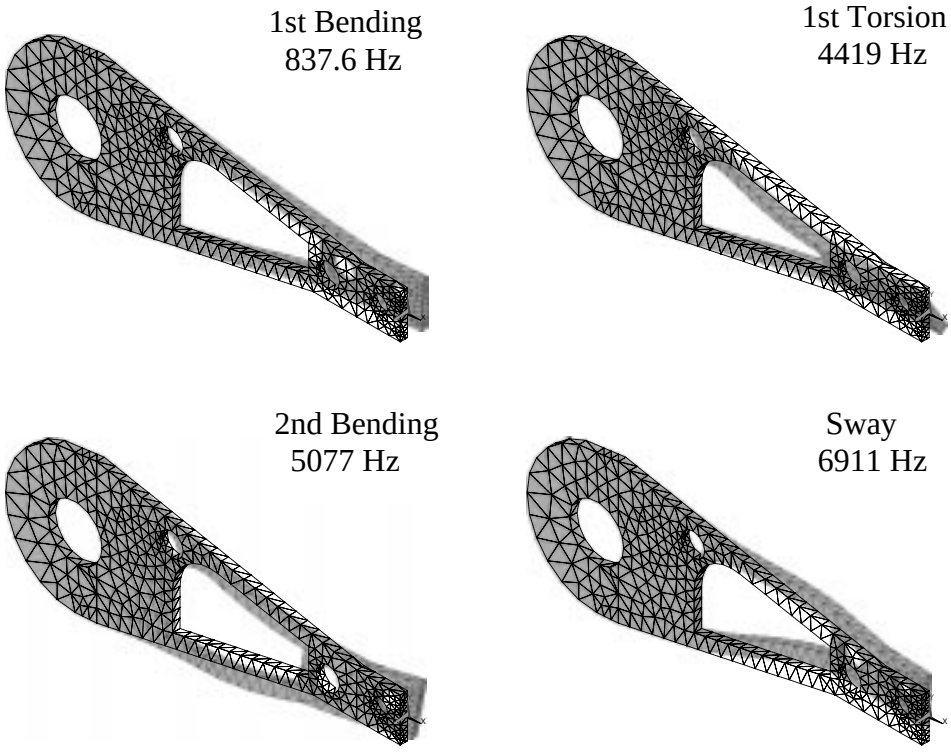

Figure 10 Analyzed modal parameters of the actuator arm

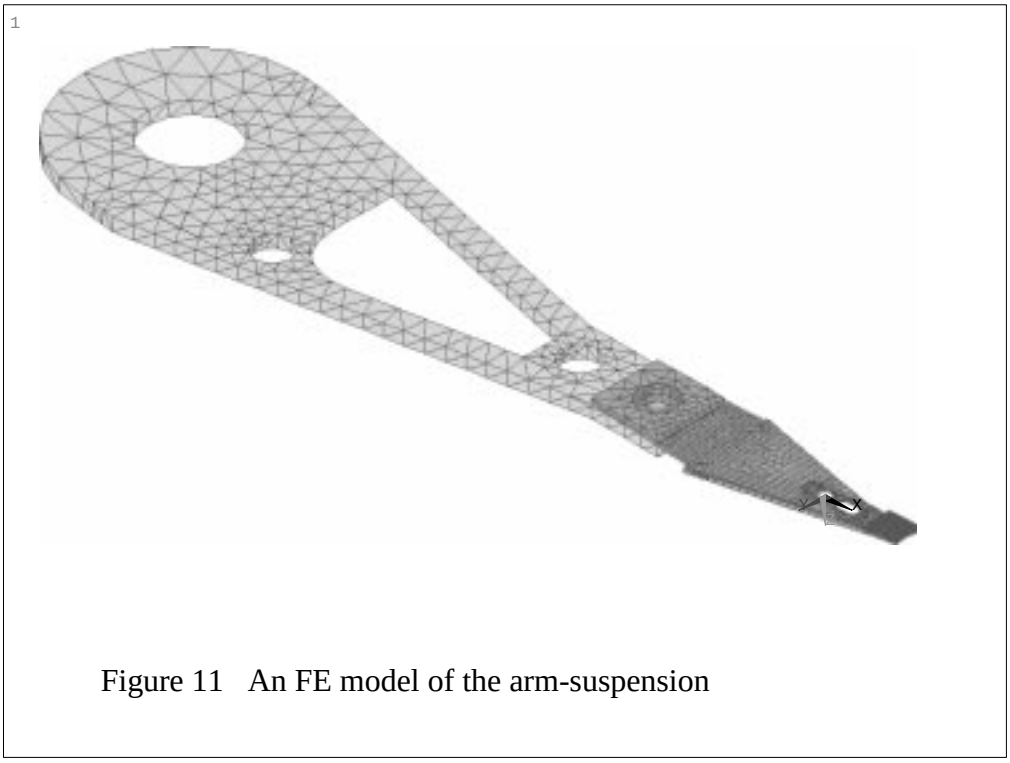

Figure 11 An FE model of the arm-suspension

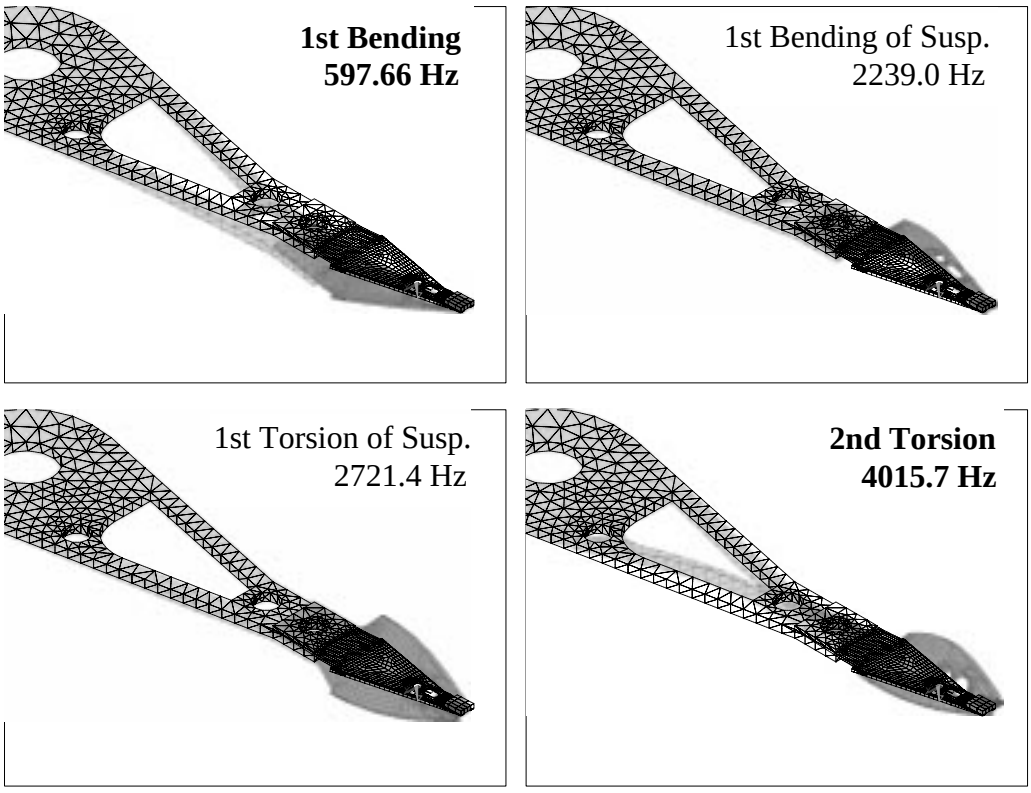

(Continued in next page)

Figure 12 Analyzed modal parameters of the arm-suspension

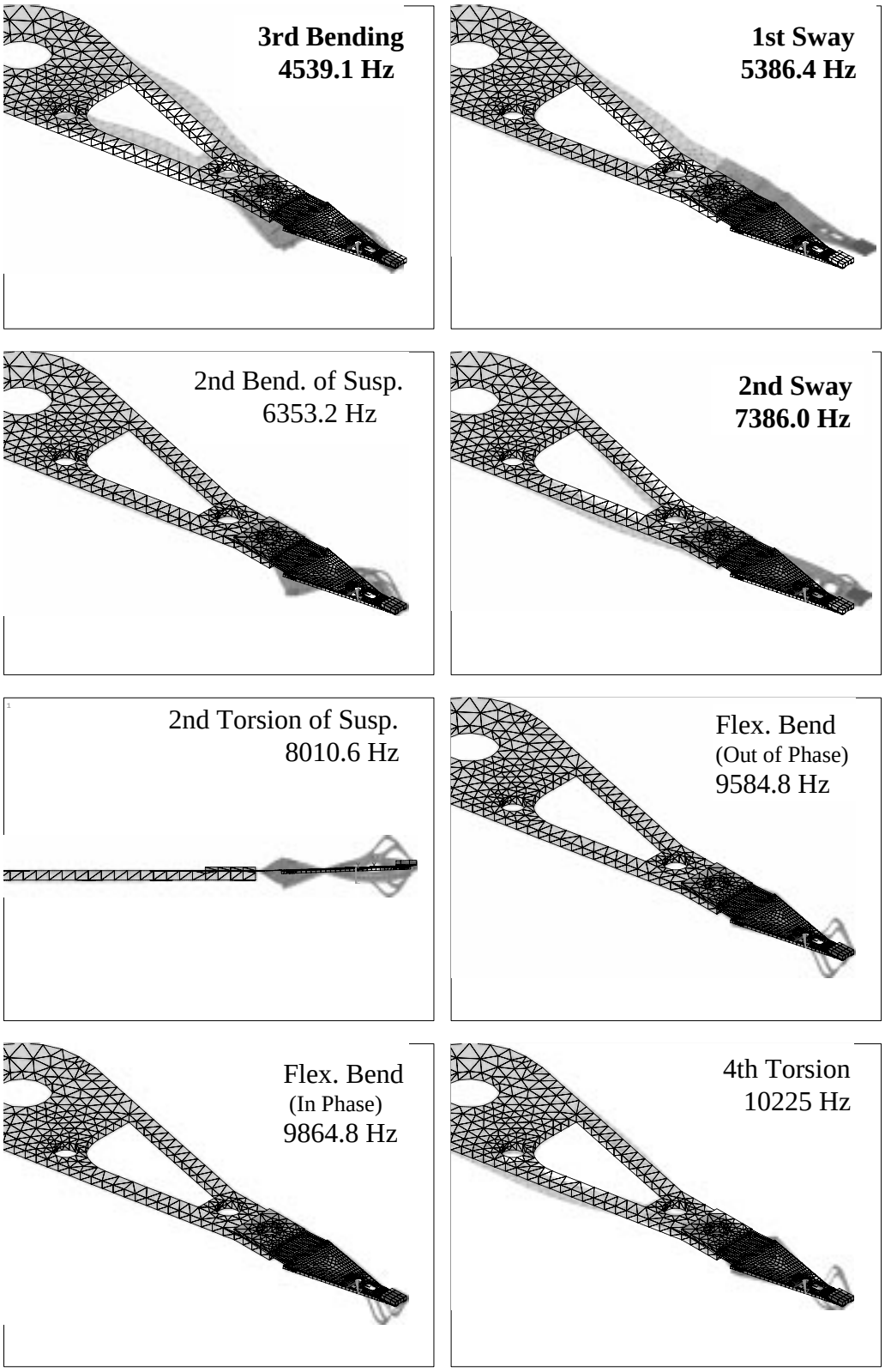

Figure 12 (Continued) Analyzed modal parameters of the arm-suspension

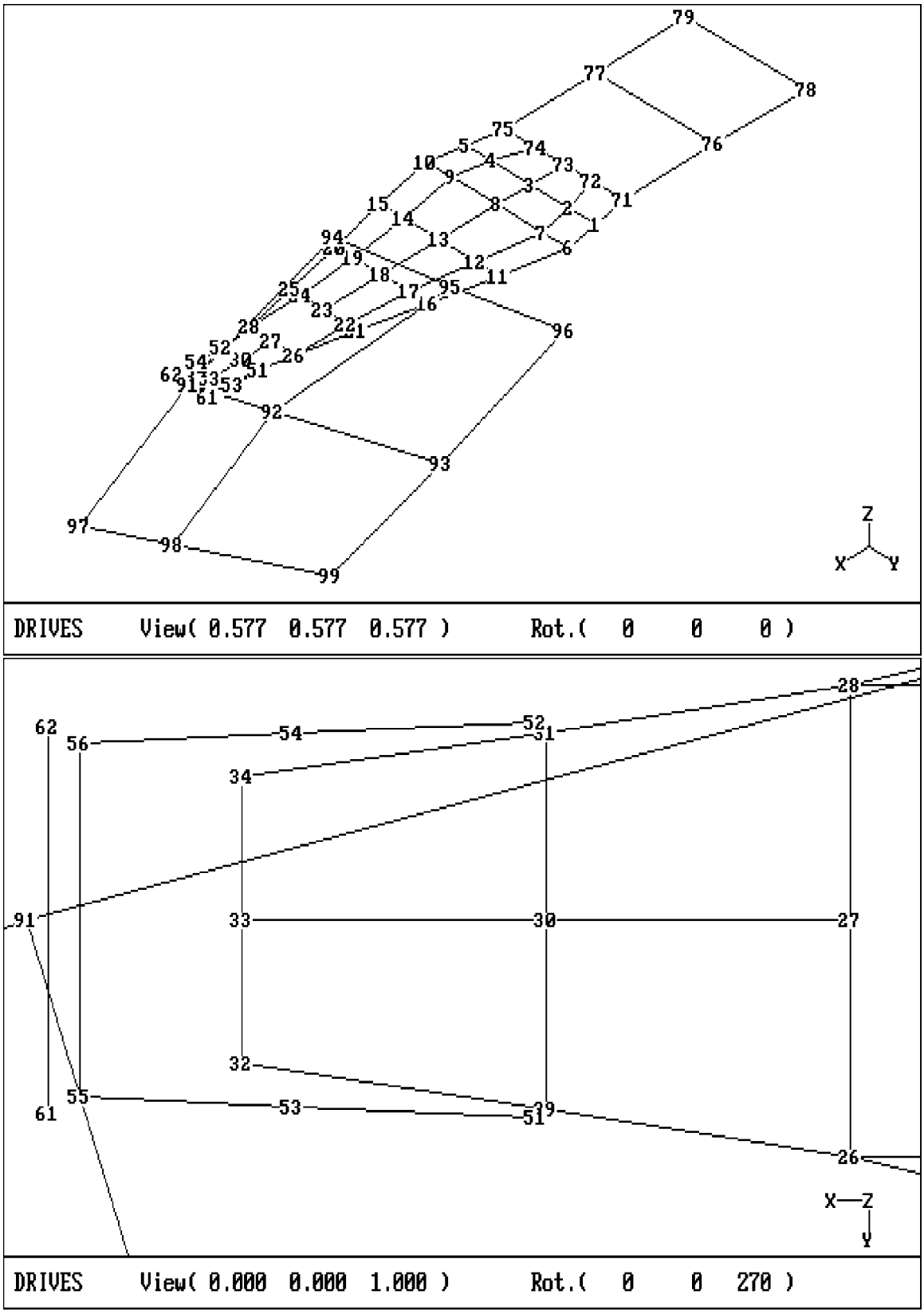

Figure 13 Geometric model used in the experiment of the drive with stationary disks

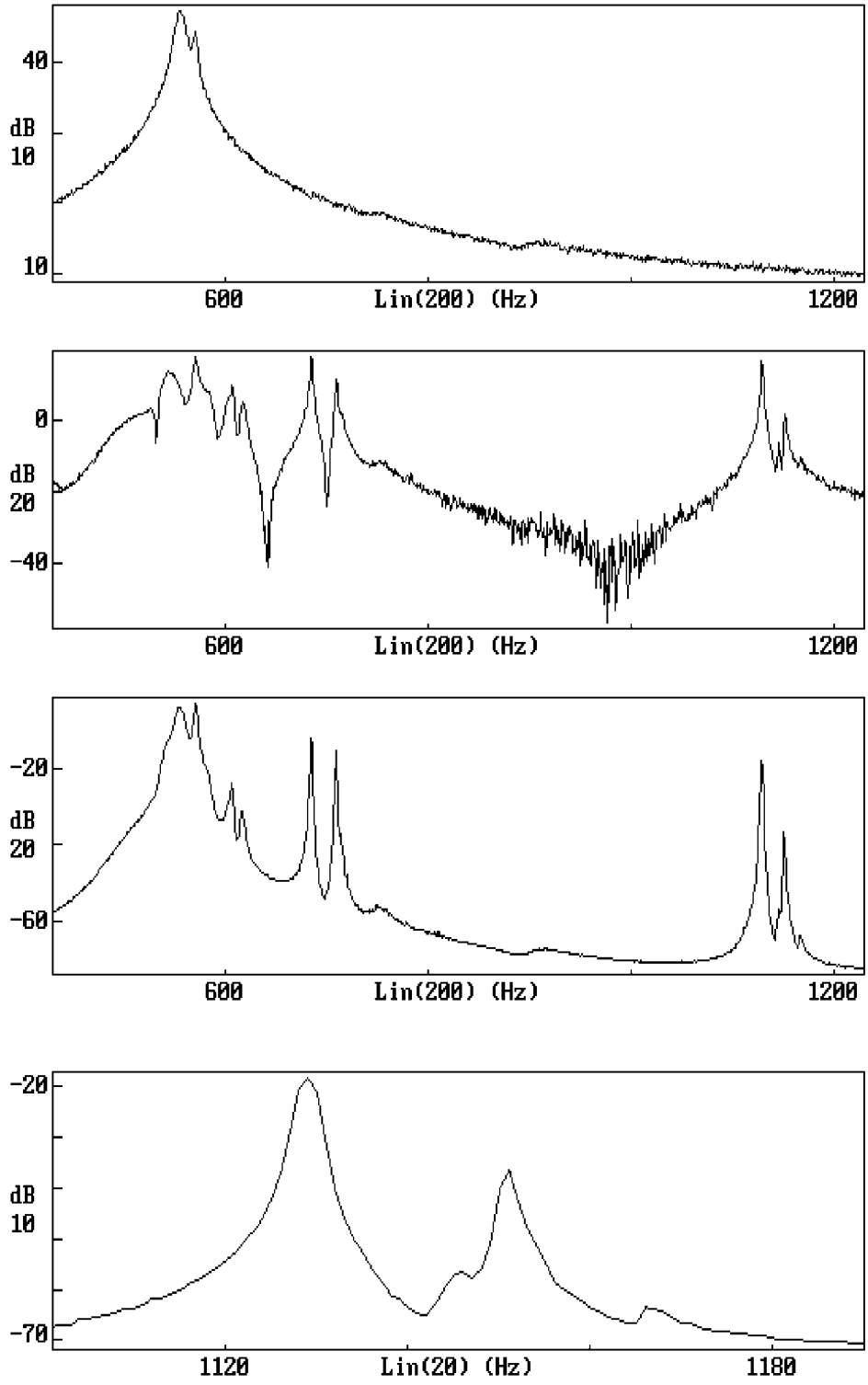

Figure 14 Measured FRFs of the drive with stationary disks in the frequency band of 420-1220

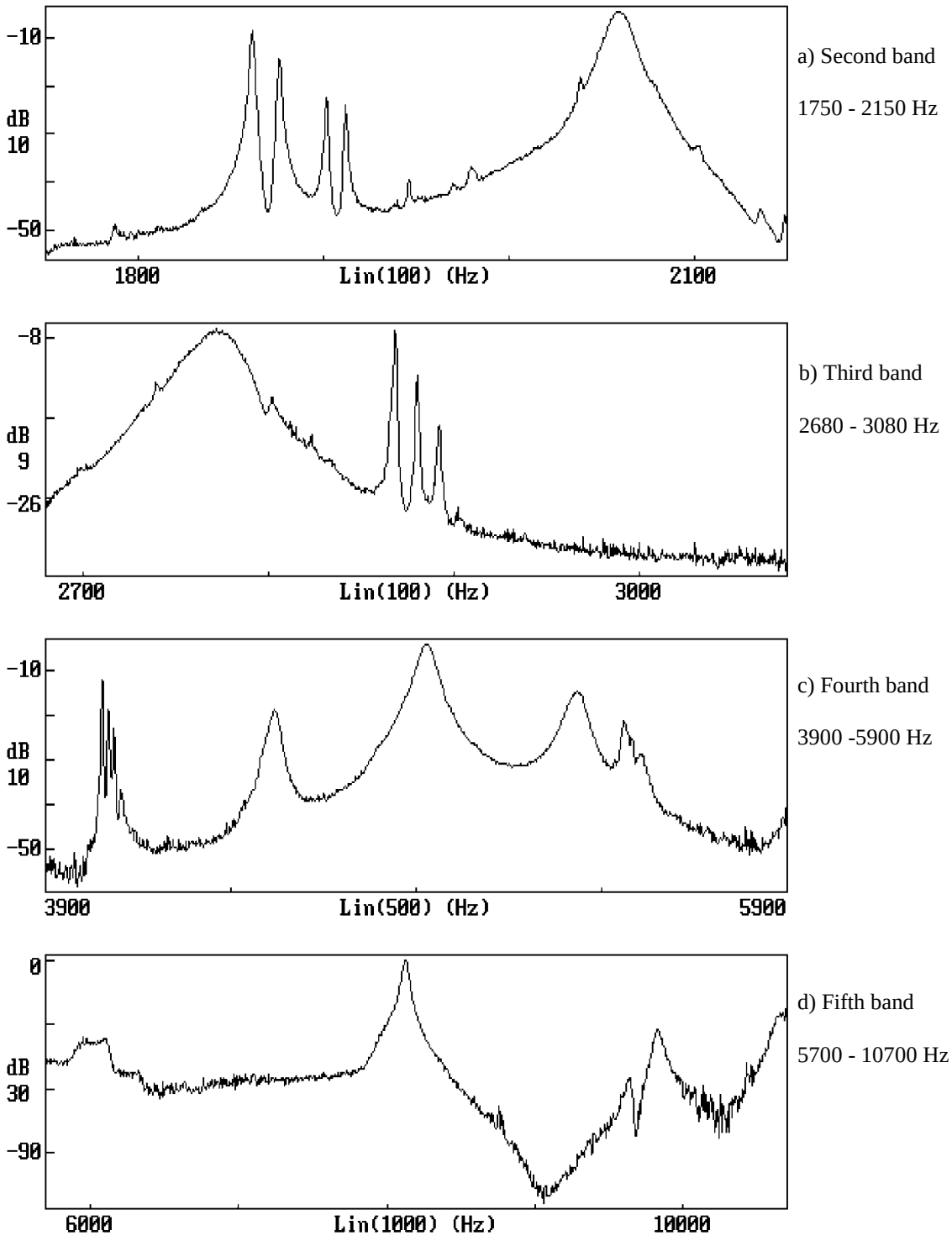

Figure 15 Averaged measured FRFs of the drive with stationary disks

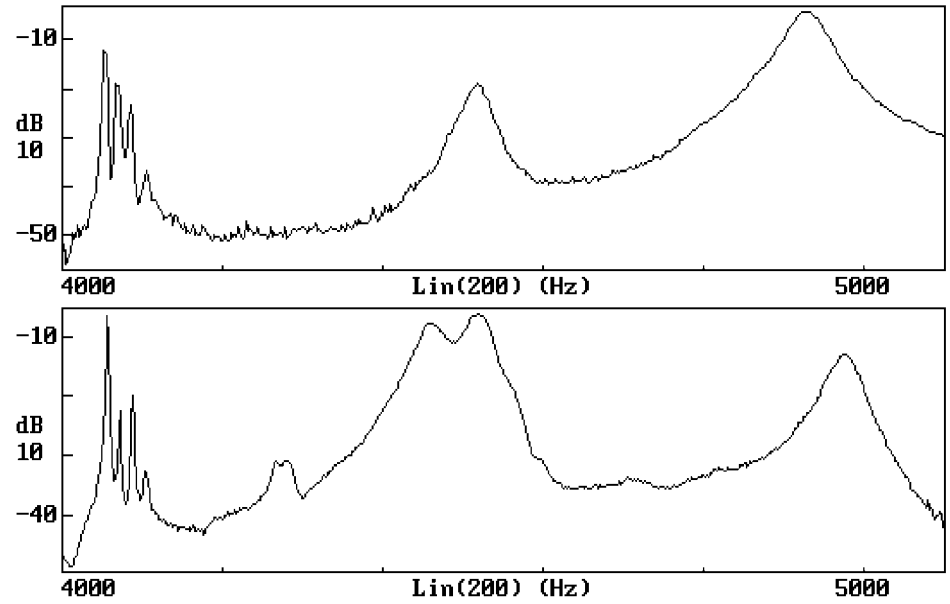

a) The first experiment

b) The second experiment

Figure 16 Averaged measured FRFs in the frequency band of 4000-5100 Hz Comparison of the two experiments

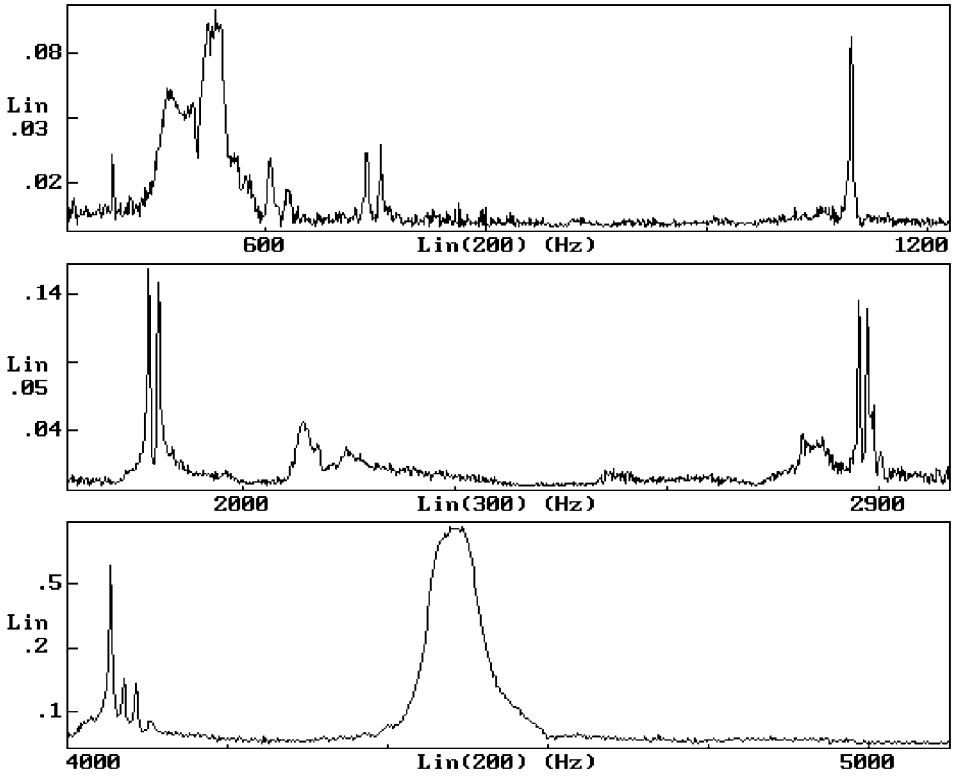

a)
420 - 1220 Hz

b)
1750 - 3000 Hz

c)
3500 - 5100 Hz

(4100-5100 Hz displayed)

Figure 17 Measured FRFs of the drive with the stationary disks on the slider in the lateral direction

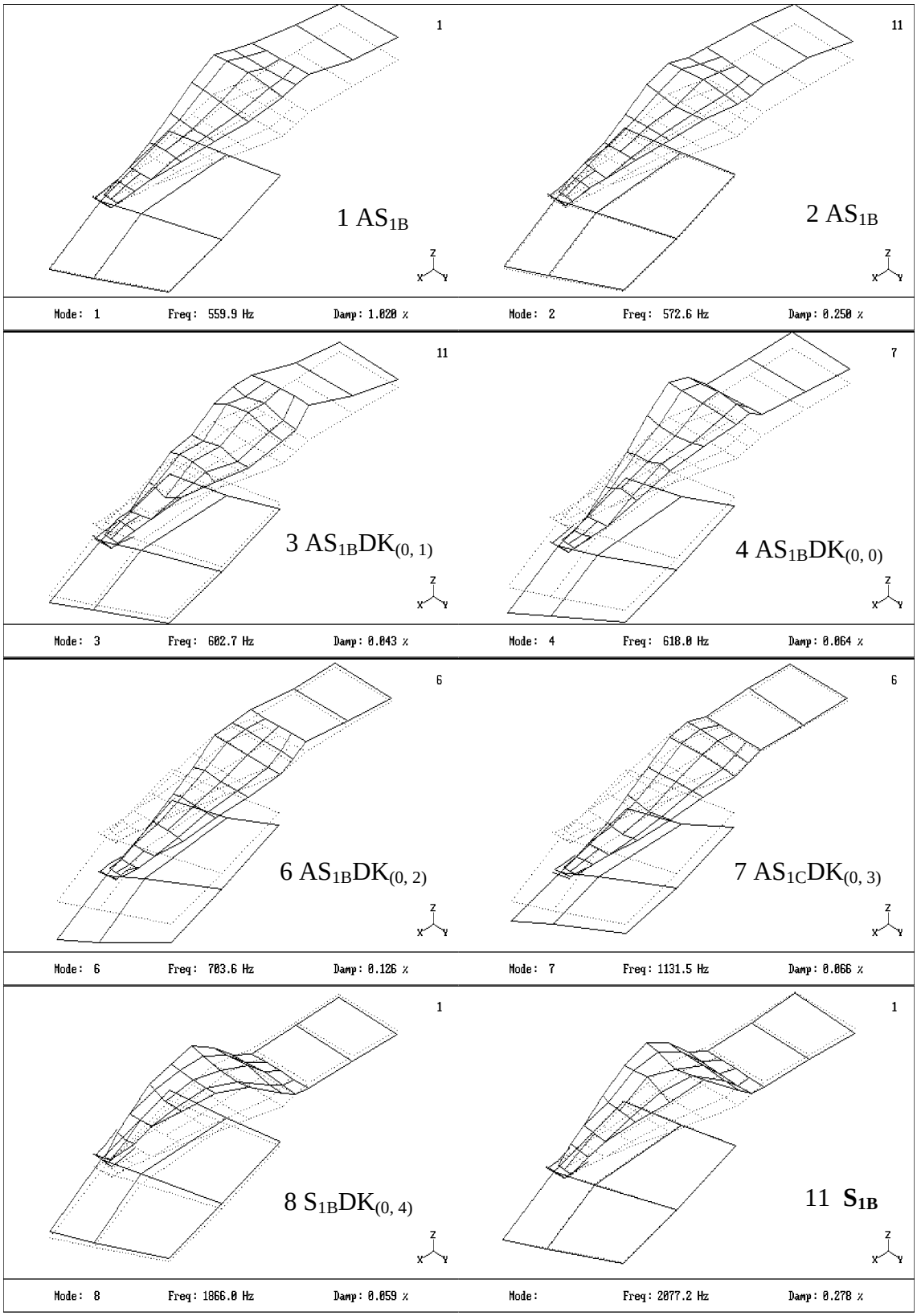

(Continued in next page)

Figure 18 Measured mode shapes of the drive with stationary disks

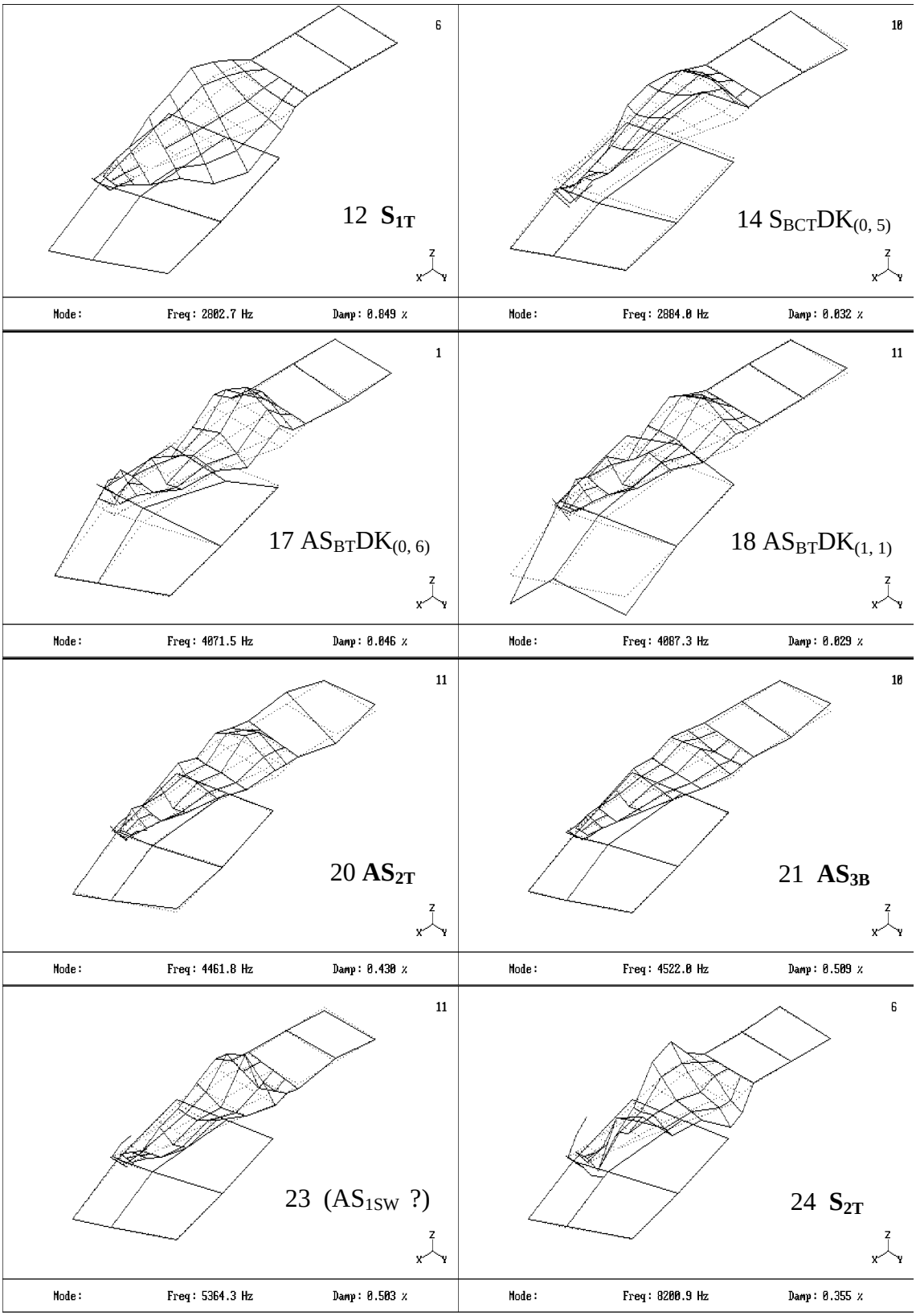

Figure 18 (Continued) Measured mode shapes of the drive with stationary disks

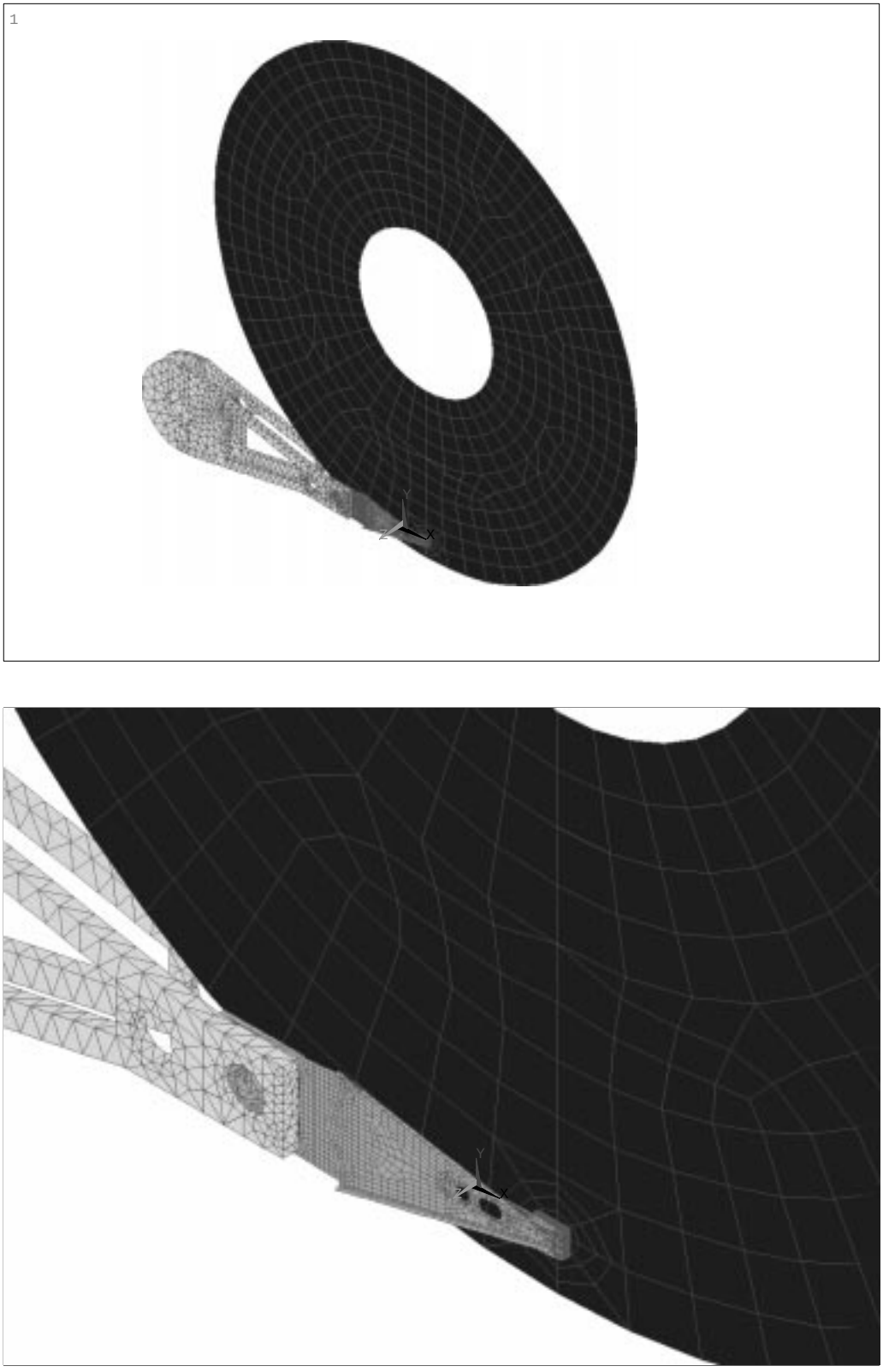

Figure 19 An FE model of the drive

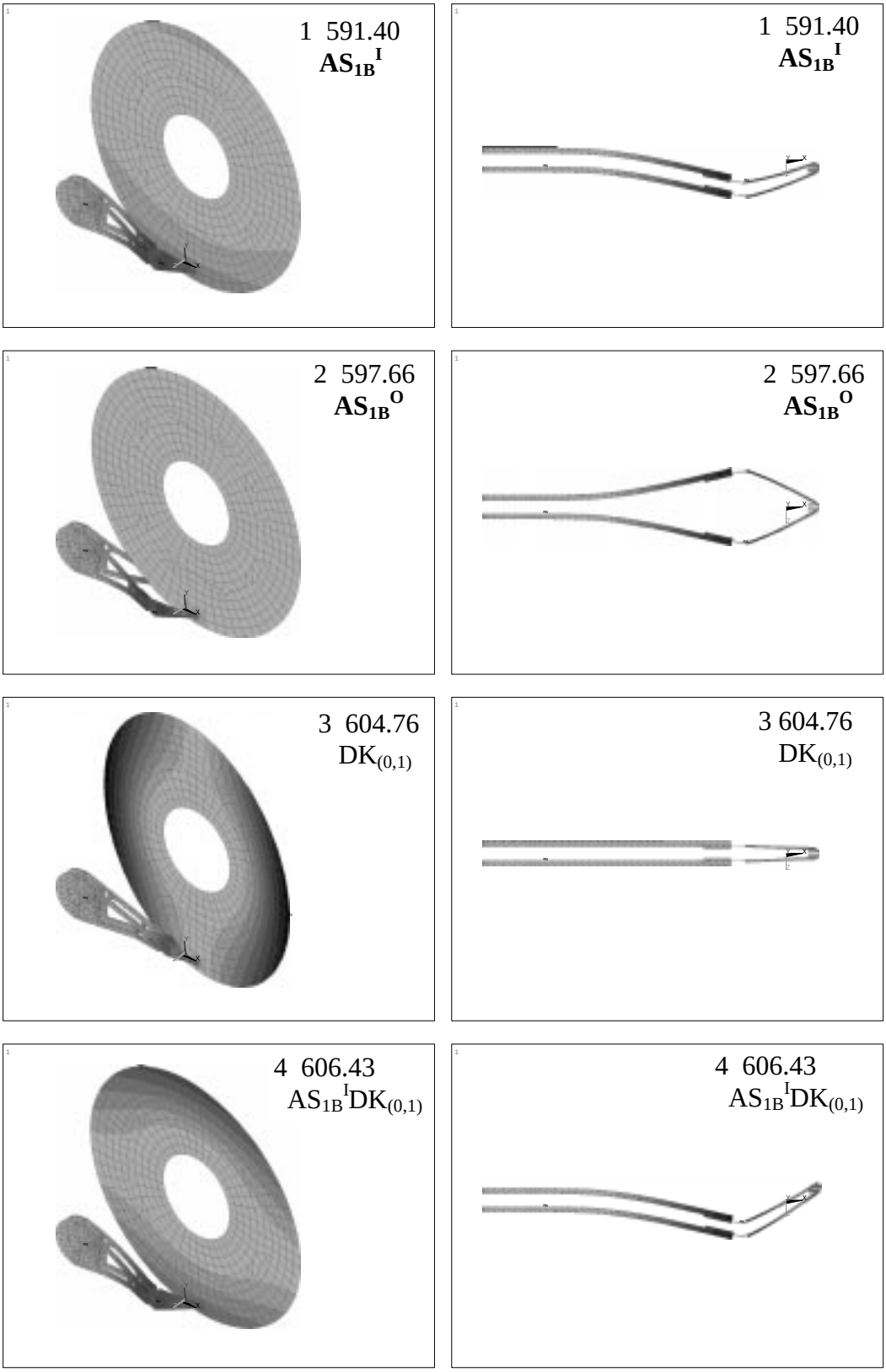

(Continued in next page)

Figure 20 Some analyzed mode shapes of the drive

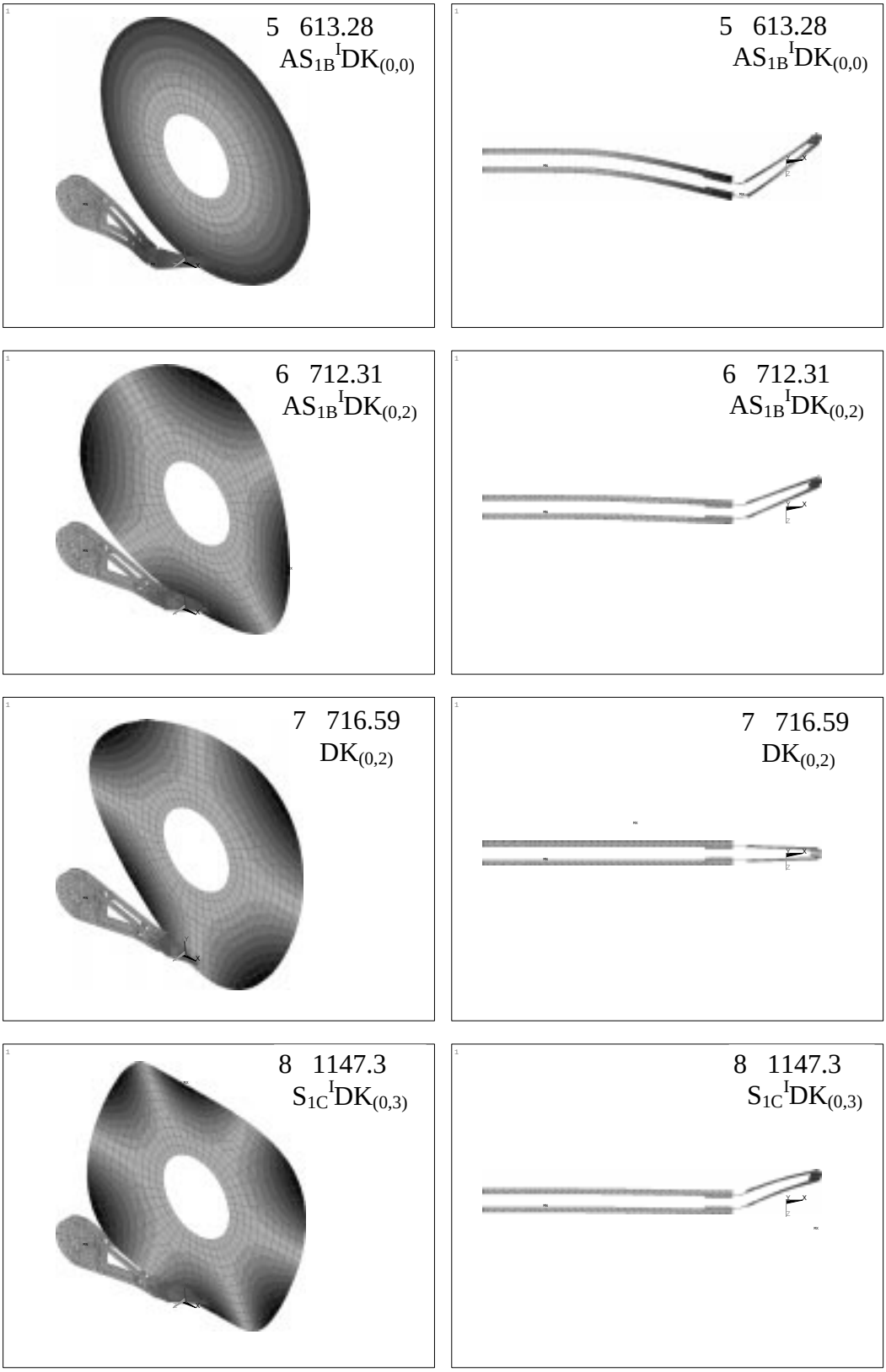

(Continued in next page)

Figure 20 (Continued) Some analyzed mode shapes of the drive

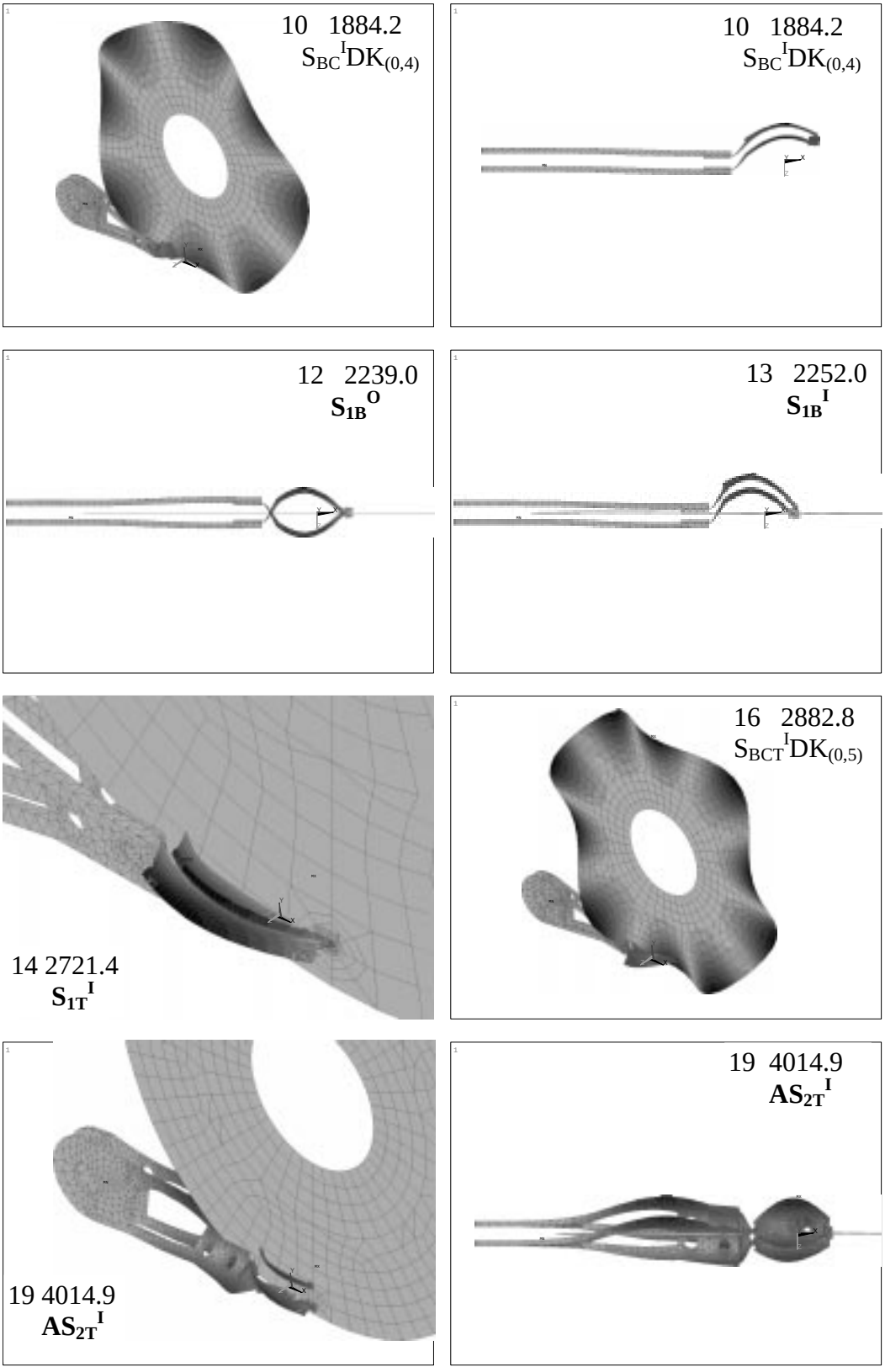

(Continued in next page)

Figure 20 (Continued) Some analyzed mode shapes of the drive

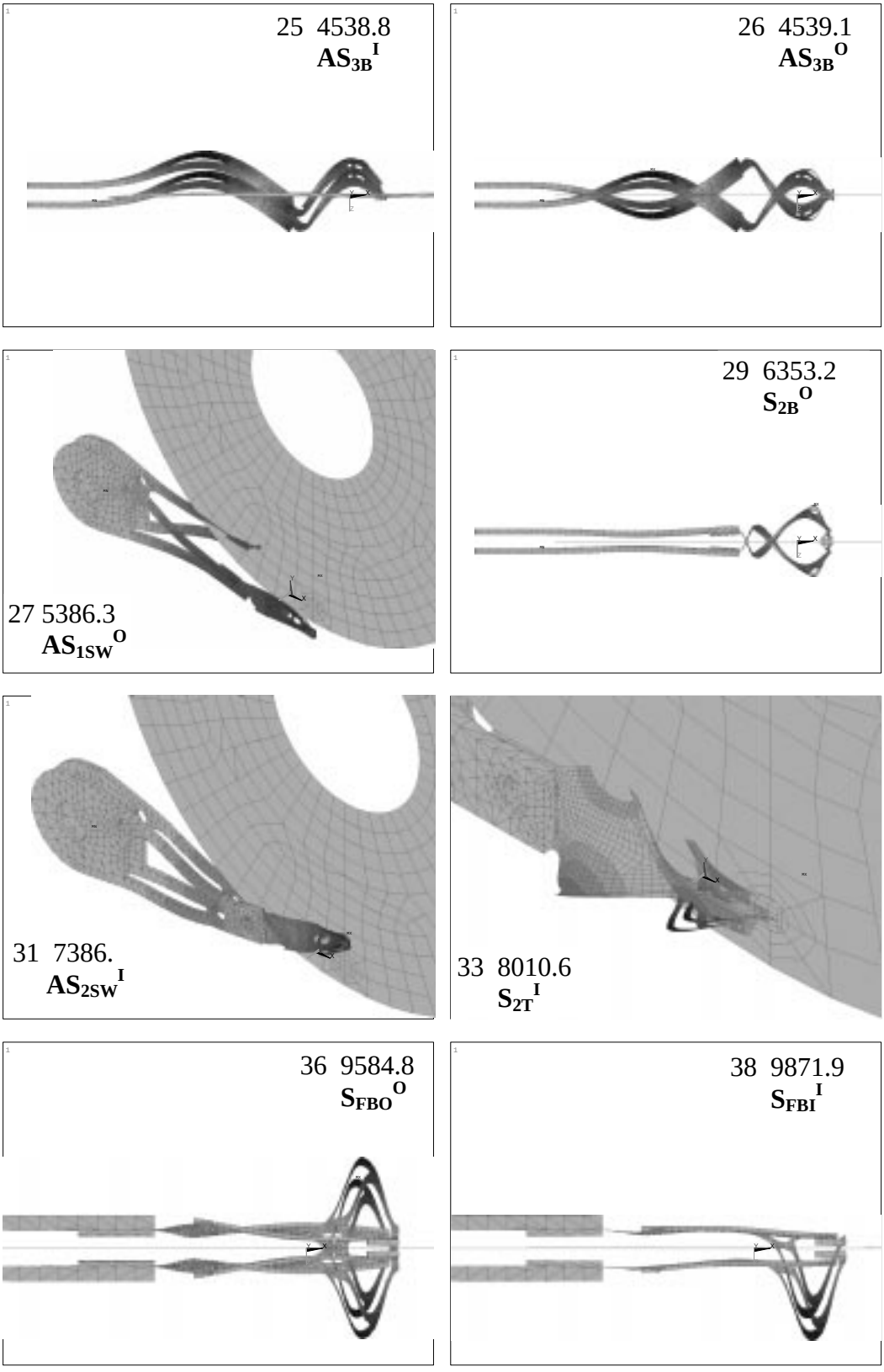

Figure 20 (Continued) Some analyzed mode shapes of the drive

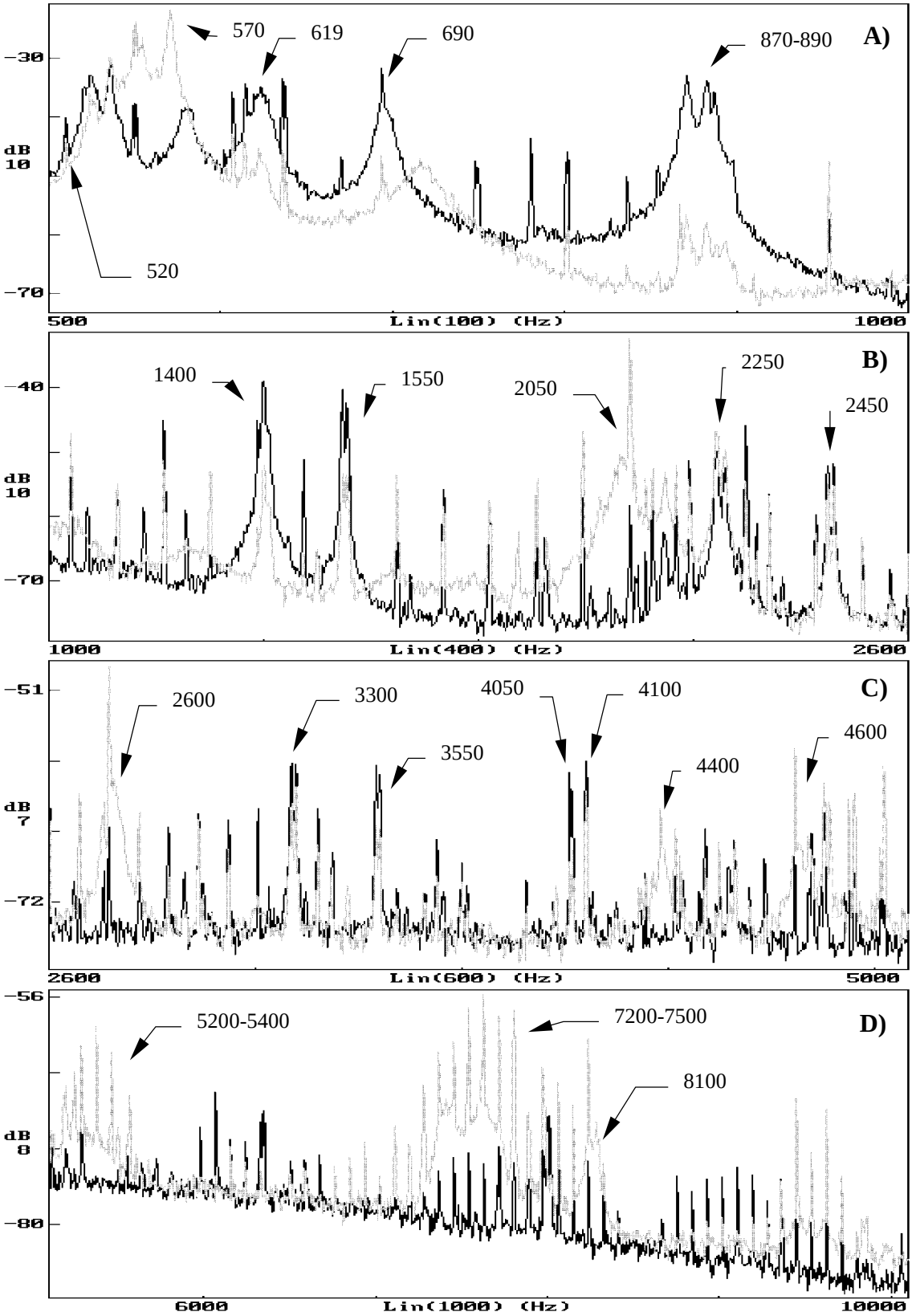

Figure 21 Measured power spectra (Z direction) of the drive with rotating disks
——— at the slider ····· at the suspension point 6)

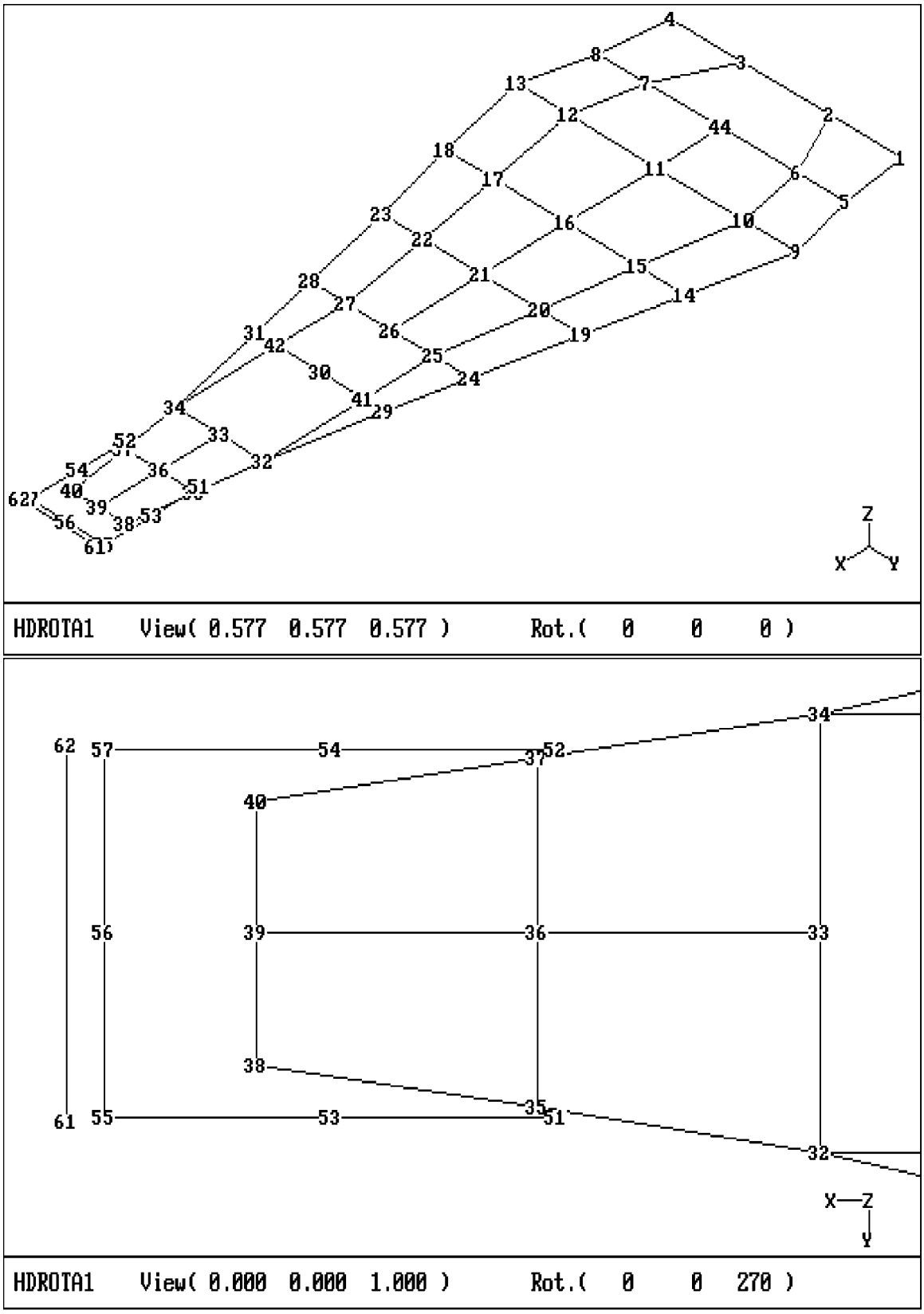

Figure 22 Geometric model used in the experiment of the drive with rotating disks

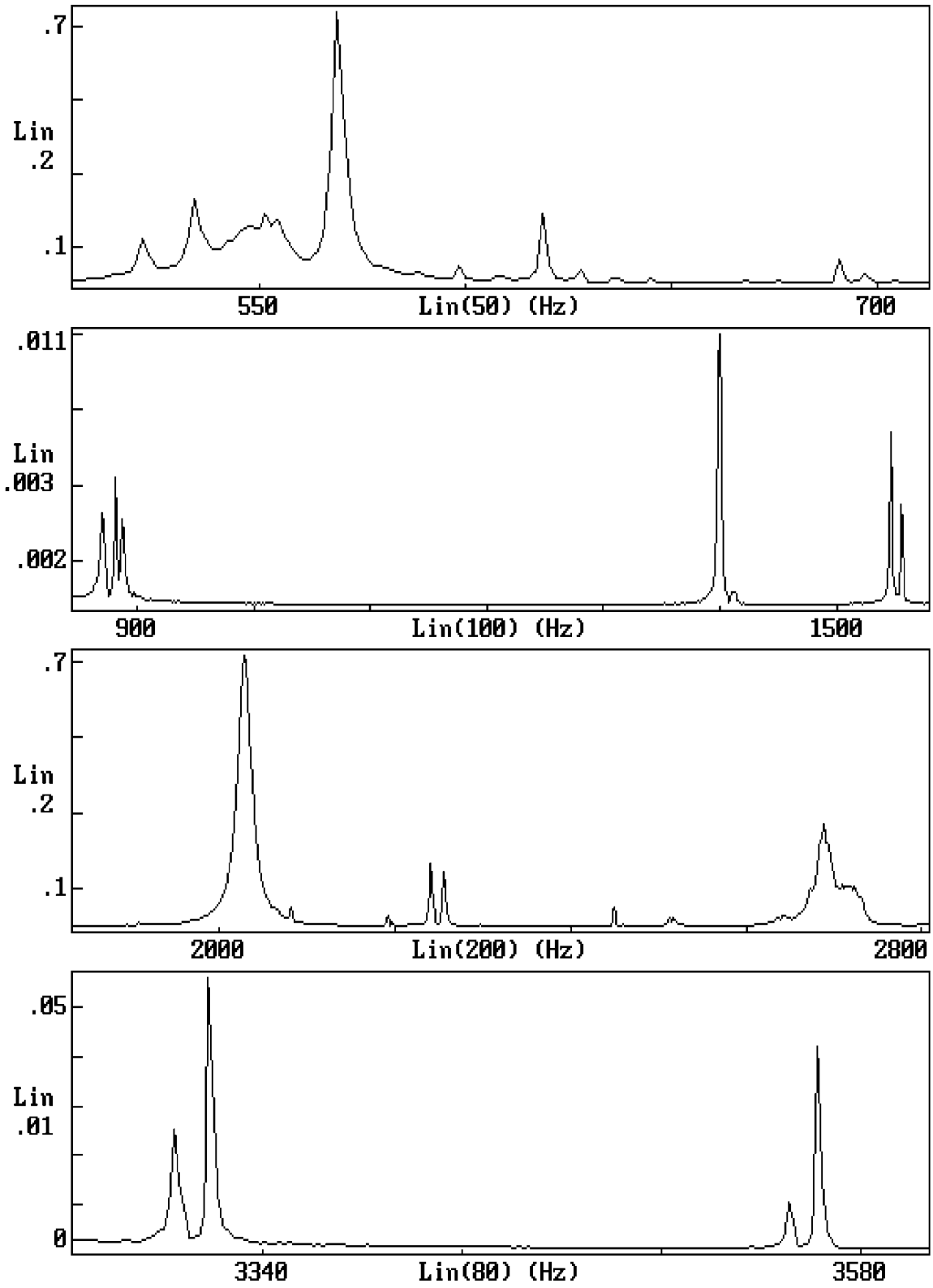

Figure 23 Measured averaged FRFs of the drive with rotating disks in the different bands

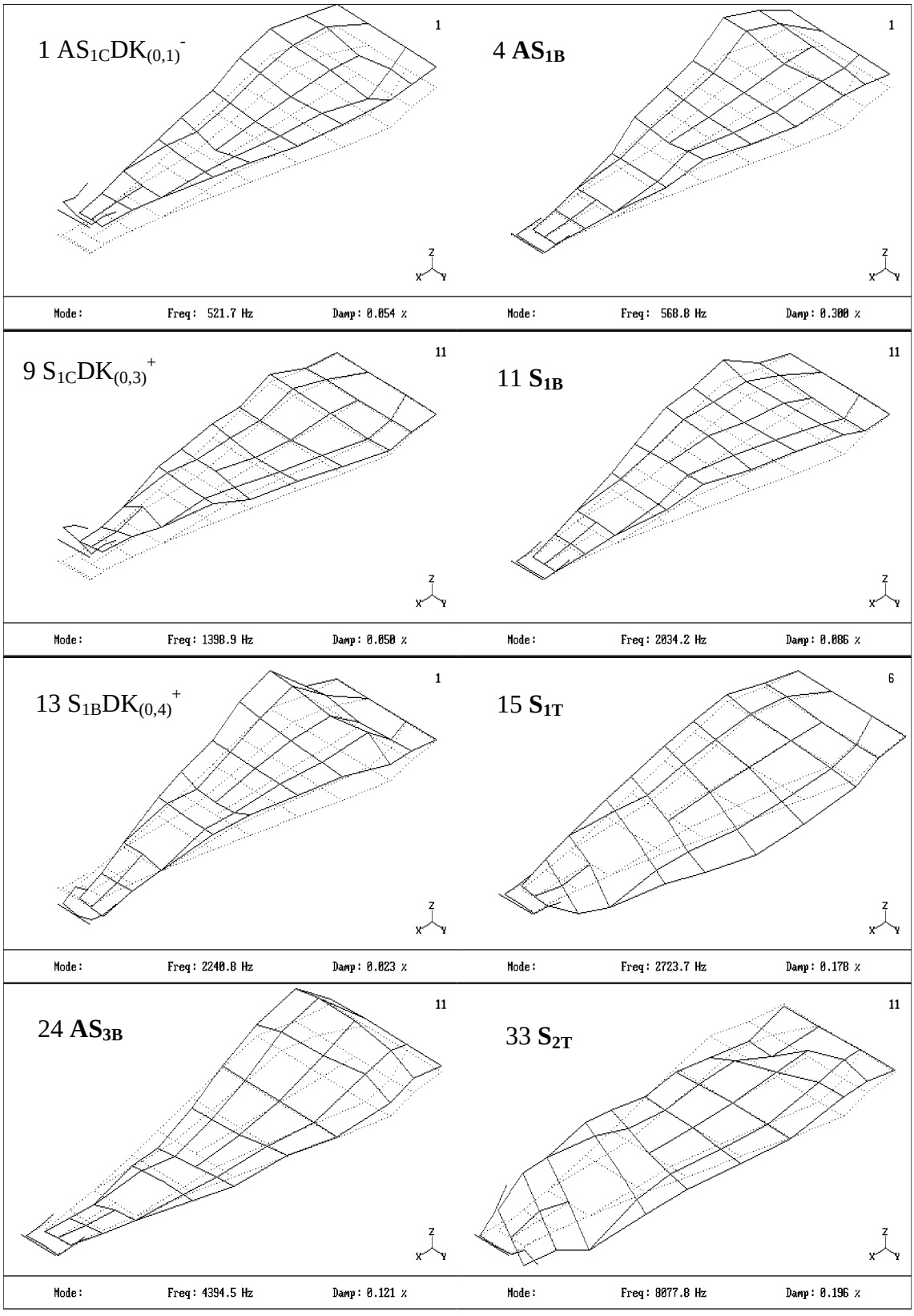

Figure 24 Some measured mode shapes of the drive with rotating disks

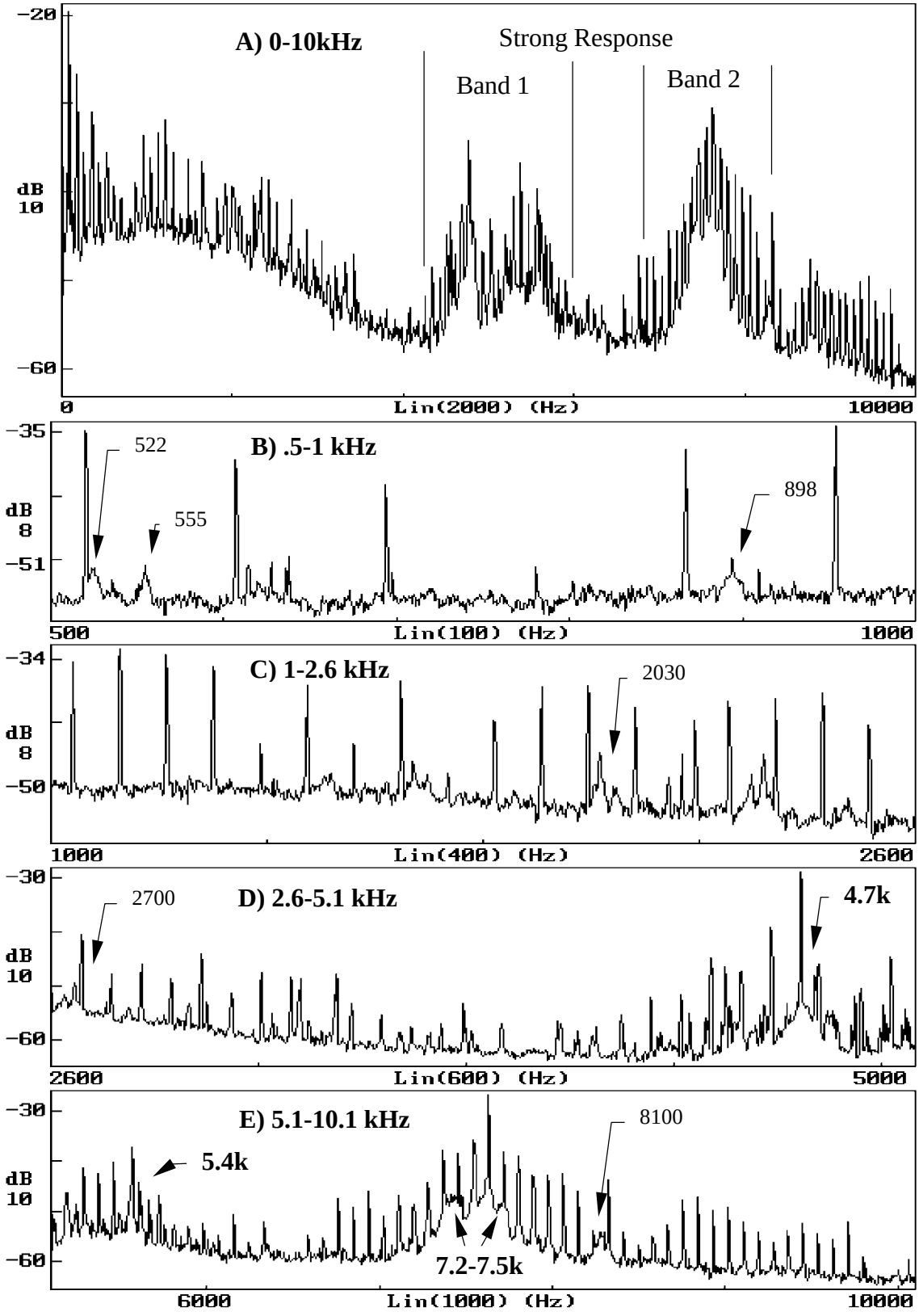

Figure 25 Measured PSDs of velocity responses of the slider in the lateral direction